Decomposed Discrete-Time Model and Multiscale Oscillations Analysis of the DAB Converter

Guoqing Gao, *Student Member, IEEE*, Wanjun Lei, *Member, IEEE*, Qibo Tang, Zhongxiu Xiao, Xiufang Hu, and Yue Wang, *Member, IEEE*

***Abstract*—A decomposed discrete-time model of the dual active bridge (DAB) converter is proposed in this article, which has significantly simplified the conventional discrete-time model without affecting the calculation accuracy of the exponential matrix. Therefore, the decomposed discrete-time model is also applied to the design of the digital controller to compensate the digital control delay, which could deteriorate the stability of the system. Besides, the comprehensive and systematic analysis of all the possible unstable phenomena of the DAB converter is conducted to reveal their intrinsic mechanism. The corresponding multiscale oscillations and the sudden jump phenomena are also presented to exhibit their dynamic characteristics. In addition, the closed-form expressions of the state variables are obtained, which are utilized to explicitly express the analytical relationships among the state variables, system parameters, and the Floquet multipliers. Accordingly, the parameter spaces of the selected crucial system parameters are obtained, which can provide the guidance for the parameters design of the DAB converter.**

***Index Terms*—Decomposed discrete-time model, digital control, dual active bridge (DAB) converter, multiscale oscillations.**

I. Introduction

THE dual-active-bridge (DAB) converter is a prominent isolated topology, which can realize the bidirectional power transfer and voltage matching [1]. With the development of the distributed generation [2], [3] and energy storage [4]–[7], the DAB converter has been a research focus with the characteristics of high efficiency, high power density, simple structure and flexible control. As a pivotal interface, the DAB converters are also widely applied to the solid-state transformers [8], [9], electric or hybrid vehicles [10]–[13] and the uninterruptible power supplies [14].

However, the parasitic nonlinear effects are inevitable in the DAB converter because of the digital control delay and the switching modes of the power switches [15], [16], which could result in some undesired oscillations and other unexpected unstable phenomena [17]–[19]. The corresponding fast-scale subharmonic oscillation, slow-scale low-frequency oscillation and the sudden jump phenomena will lead to the large ripples in the state variables or the undesired current and voltage levels, which could increase the devices stress, decrease their reliability or even damage the DAB converter and its interconnected equipment. Therefore, it is essential to apply the effective modeling methods and analyzing tools to reveal the dynamic behaviors of the DAB converter.

The conventional state-space averaging method [20] is widely applied to the modeling of the converters [21]. However, the small ripple hypothesis no longer holds in the DAB converter because the inductor current is the pure ac component. Therefore, the generalized average model of the DAB converter is proposed in [22]. Since only the dc term and first-order terms of the inductor current are utilized, the precision of this continuous-time model is quite low especially when there are large harmonic distortions. There are also the reduced-order average model [23], [24] and inductor current average model [25], [26] proposed to avoid the ac inductor current. However, the averaged output inductor current will inevitably lose the fast-scale dynamics of the inductor current. What is more, the reduced-order average model completely loses the inductor current dynamics. Since the continuous-time average model of the DAB converter cannot unfold the fast switching-frequency scale dynamics of the inductor current, many works about the discrete-time model have been proposed. According to the discrete-time modeling method of the non-isolated dc–dc converters [27], the discrete-time small-signal model of the DAB converter is also developed in [28]. The discrete-time small-signal models in [16] and [29] are accurate up to 1/3 and 1/10 of the switching frequency as shown in [26]. Based on the half-cycle symmetry characteristics of the state variables, the discrete-time models [30], [31] are proposed, which are suitable for the modeling of the half-cycle delay control. Besides, the bilinear discrete-time model of the DAB converter is proposed in [17] to simplify the complex exponential matrices iteration. However, the bilinear approximation is based on the first-order Taylor approximation of the stable operating point, which restricts the transient characteristics of the DAB converter [31].

In this article, the decomposed discrete-time model of the DAB converter is proposed. The discrete-time model has been simplified without affecting the calculation accuracy of the exponential matrix compared with the conventional discrete-time iteration [17], [32], [33]. Therefore, the decomposed discrete-time

Manuscript received June 20, 2019; revised October 3, 2019 and December 16, 2019; accepted January 12, 2020. Date of publication January 28, 2020; date of current version May 1, 2020. This work was supported by the National Key Research & Development Plan under Grant 2018YFB0905800. Recommended for publication by Associate Editor D. Xu. *(Corresponding author: Wanjun Lei.)*

The authors are with the State Key Laboratory of Electrical Insulation and Power Equipment, Shaanxi Key Laboratory of Smart Grid, School of Electrical Engineering, Xi'an Jiaotong University, Xi'an 710049, China (e-mail: gaoguoqing@stu.xjtu.edu.cn; leiwanjun@mail.xjtu.edu.cn; 564388442@qq.com; xiao_zhongxiu@163.com; huxiufang029@stu.xjtu.edu.cn; davidwangyue@mail.xjtu.edu.cn).

Color versions of one or more of the figures in this article are available online at http://ieeexplore.ieee.org.

Digital Object Identifier 10.1109/TPEL.2020.2970039

model is applied to the design of the digital controller to compensate the digital control delay, which could deteriorate the stability of the system. According to the decomposed discrete-time model of the DAB converter, the closed-form expressions of the state variables are also obtained, which can be utilized to explicitly express the analytical relationships among the state variables and the system parameters. Besides, only the slow-scale oscillation of the DAB converter under the proportional control is analyzed in [17] and [32]. However, the fast-scale subharmonic oscillation and sudden jump phenomena of the DAB converter are very common in the practical applications. Therefore, the comprehensive and systematic analysis of these different kinds of unstable phenomena is conducted to reveal their underlying mechanism according to the decomposed discrete-time model. The relationships among the system parameters, state variables, and the Floquet multipliers are also revealed analytically based on the proposed discrete-time correlation factor, sensitivity analysis and the Gershgorin bands analysis. Accordingly, the parameter spaces of the crucial system parameters are obtained, which can provide the reliable guidance for the parameters design. However, it is also shown that the parameters design according to the conventional stability margin criteria [34], [35] cannot guarantee the stable operation of the system with sufficient stability margin.

The structure of this article is as follows. The system description and the decomposed discrete-time model of the DAB converter are presented in Section II. Then, in Section III, the characteristics of the multiscale oscillations are described in detail. In Section IV, the mechanism of the multiscale oscillations and other unstable phenomena are investigated systematically. Besides, the parameters design methods are also proposed to prevent these different kinds of unstable phenomena. The experimental results are also illustrated in Section V to verify the analysis and the simulation results. Finally, the conclusion is drawn in Section VI.

II. System Description and Decomposed Discrete-Time Modeling

A. System Description

The DAB converter prototype studied in this article will be utilized in a bidirectional power flow application, where the input of the DAB converter is an infinite dc bus and the output is the energy storage device when operating in the forward direction. The diagram of the digitally controlled DAB converter is shown as Fig. 1. The controllable power switches S_1–S_8 make up the two H bridges, which are interfaced through the magnetic network. The magnetic network is composed of the external auxiliary inductor and the high-frequency transformer with the turns ratio of n. L is the sum of the external inductance and the equivalent leakage inductance of the transformer. V_1 and V_2 are the input and output voltage, respectively. $R_{\rm eq}$ is the sum of the winding resistance and the ON-resistance of switching devices. The magnetic network provides not only the galvanic isolation but also the voltage matching and the energy storage. Besides, the phase-shift modulation is applied to the digital controller.

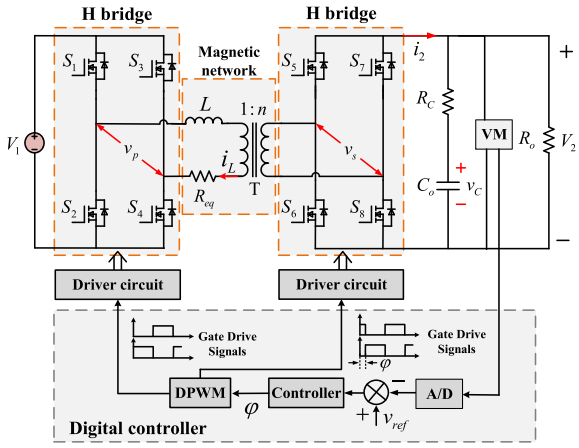

Fig. 1. Diagram of the digitally controlled DAB converter.

The phase-shift modulation is the most popular modulation method for the nonresonant DAB converters. The modulation techniques of the phase-shift modulation mainly include the single-phase-shift (SPS), extended-phase-shift (EPS), dual-phase-shift (DPS), and the triple-phase-shift (TPS) modulation. In this article, the most widely used SPS modulation is applied to the DAB converter for the sake of simplicity. The operation waveforms in the steady state are illustrated in Fig. 2. The ac voltage v_p and v_s of the magnetic network terminals are phase-shifted according to the phase shift angle φ_n in each switching cycle. Therefore, there are four subintervals with the length of t_{ni} $(i = 1, 2, 3, 4)$ in each switching cycle (the influence of dead band [36], [37] is not considered in this article). Besides, the state variables i_L and v_C are symmetric within a switching cycle.

B. Decomposed Discrete-Time Modeling

1) Power Circuit Modeling: Because the switches of the H bridges periodically change their configurations, the DAB converter toggles between four circuit topologies in one switching cycle. According to the circuit structure and operating principle of each circuit topology, the state equation of the *i*th subinterval with the *i*th topology can be obtained as

$$\dot{\mathbf{x}} = \mathbf{A}_i\mathbf{x} + \mathbf{B}_i V_1, i = 1, 2, 3, 4 \tag{1}$$

where $\mathbf{x}$ represents the state vector, which is comprised of the inductor current i_L and the output capacitor voltage v_C. V_1 is the input voltage of the DAB converter. Besides, the system matrix $\mathbf{A}_i$ and vector $\mathbf{B}_i$ corresponding to each topology are expressed as follows:

$$\mathbf{A}_1 = \mathbf{A}_2 = \begin{bmatrix} -\frac{n^2R_{eq}+R_oR_C/(R_o+R_C)}{n^2L} & -\frac{R_o}{nL(R_o+R_C)} \\ \frac{R_o}{nC_o(R_o+R_C)} & -\frac{1}{C_o(R_o+R_C)} \end{bmatrix}$$
$$\mathbf{A}_3 = \mathbf{A}_4 = \begin{bmatrix} -\frac{n^2R_{eq}+R_oR_C/(R_o+R_C)}{n^2L} & \frac{R_o}{nL(R_o+R_C)} \\ -\frac{R_o}{nC_o(R_o+R_C)} & -\frac{1}{C_o(R_o+R_C)} \end{bmatrix} \tag{2}$$

$$\mathbf{B}_1 = \mathbf{B}_4 = \begin{bmatrix} \frac{1}{L} 0 \end{bmatrix}^T, \quad \mathbf{B}_2 = \mathbf{B}_3 = \begin{bmatrix} -\frac{1}{L} 0 \end{bmatrix}^T. \tag{3}$$

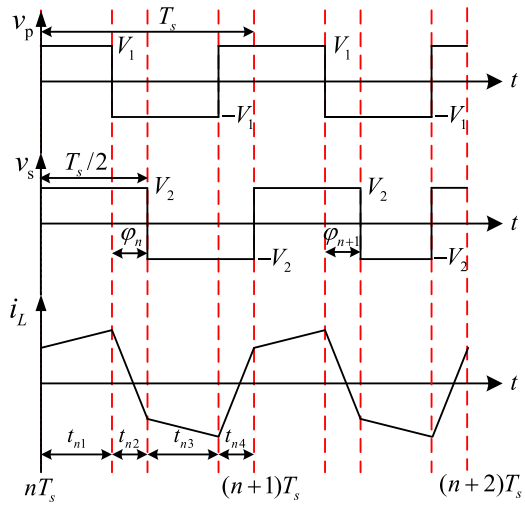

Fig. 2. Operation waveforms in the steady state.

The schematic diagram of the iterative relationship of the state vector within a switching cycle is shown in Fig. 3 under the SPS control. For the DAB converter under the DPS or TPS control, it is just required to increase the number of the subintervals from 4 to 8. According to the state equation of each subinterval, the continuous-time orbit of the state vector in each subinterval can be obtained with the fundamental theorem of calculus as shown in (4). The state vector at the end of each subinterval can be expressed by the initial state vector of the subinterval

$$\begin{aligned}\mathbf{x}_{ni} &= f_{ni}\left(\mathbf{x}_{n(i-1)}, t_{ni}\right)\\ &= \boldsymbol{\Phi}_i\left(t_{ni}\right)\mathbf{x}_{n(i-1)} + \boldsymbol{\psi}_i\left(t_{ni}\right)\end{aligned} \tag{4}$$

where $\boldsymbol{\Phi}_i(t_{ni}) = e^{\mathbf{A}_i t_{ni}}$, $\psi_i(t_{ni}) = \int_0^{t_{ni}} \boldsymbol{\Phi}_i(t)\mathbf{B}_i V_1 \mathrm{d}t$.

By combining the iterative (4) of each subinterval, the discrete-time iterative relationship between the state vector $\mathbf{x}_n$ and $\mathbf{x}_{n+1}$ of the two switching cycles is expressed as

$$\begin{aligned}\mathbf{x}_{n+1} &= f\left(\mathbf{x}_n, \varphi_n\right)\\ &= \boldsymbol{\Phi}_T\mathbf{x}_n + \psi_T\left(\varphi_n\right)\end{aligned} \tag{5}$$

where

$$\begin{aligned}\boldsymbol{\Phi}_T &= \prod_{i=4}^{1}\boldsymbol{\Phi}_i\left(t_{ni}\right)\\ \psi_T\left(\varphi_n\right) &= \sum_{j=1}^{3}\left(\left(\prod_{i=4}^{j+1}\boldsymbol{\Phi}_i\left(t_{ni}\right)\right)\psi_j\left(t_{nj}\right)\right) + \psi_4\left(t_{n4}\right)\\ t_{n1} &= t_{n3} = T_s/2 - \varphi_n T_s/2\pi,\ t_{n2} = t_{n4} = \varphi_n T_s/2\pi.\end{aligned} \tag{6}$$

The discrete-time iterative expression (5) is quite complicated, which is difficult to be applied to the digital controller. Besides, the discrete-time iterative process is based on the iteration of the state vector and the product of the matrix exponentials. It is inconvenient to analytically express the relationship among the

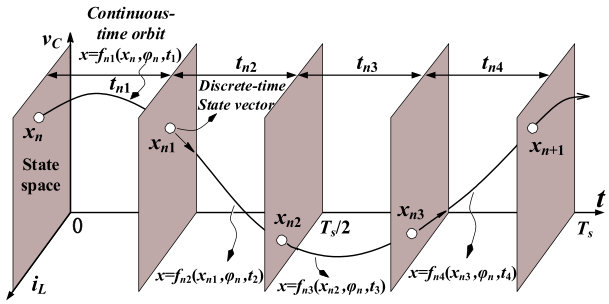

Fig. 3. Iterative relationship of the state vector within a switching cycle.

state variables and the relationship among the system parameters and the state variables. Therefore, the modal decomposition is applied to the matrix exponential as shown in (7), where μ and $\boldsymbol{\nu}$ are the matrices composed by the right and left eigenvectors of the system matrix $\mathbf{A}_3$, respectively

$$\begin{aligned}&e^{\mathbf{A}_3 T_s/2\pi}\\ &= \boldsymbol{\mu}\begin{bmatrix}e^{\lambda_1} & 0\\ 0 & e^{\lambda_2}\end{bmatrix}\boldsymbol{\nu} = \begin{bmatrix}\mu_{11} & \mu_{12}\\ \mu_{21} & \mu_{22}\end{bmatrix}\begin{bmatrix}e^{\lambda_1} & 0\\ 0 & e^{\lambda_2}\end{bmatrix}\begin{bmatrix}\nu_{11} & \nu_{12}\\ \nu_{21} & \nu_{22}\end{bmatrix}\\ &= \begin{bmatrix}\mu_{11}\nu_{11}e^{\lambda_1} + \mu_{12}\nu_{21}e^{\lambda_2} & \mu_{11}\nu_{12}e^{\lambda_1} + \mu_{12}\nu_{22}e^{\lambda_2}\\ \mu_{21}\nu_{11}e^{\lambda_1} + \mu_{22}\nu_{21}e^{\lambda_2} & \mu_{21}\nu_{12}e^{\lambda_1} + \mu_{22}\nu_{22}e^{\lambda_2}\end{bmatrix}.\end{aligned} \tag{7}$$

Define the function $\sigma(x, y, z) = \mu_{yx}\nu_{xz}$, then

$$\begin{aligned}\mathbf{H}\left(\varphi\right) &= e^{\varphi\mathbf{A}_3 T_s/2\pi}\\ &= \begin{bmatrix}\rho\left(\varphi,1,1\right) & \rho\left(\varphi,1,2\right)\\ \rho\left(\varphi,2,1\right) & \rho\left(\varphi,2,2\right)\end{bmatrix}\\ \rho\left(\varphi,a,b\right) &= \left[e^{\varphi\lambda_1}, e^{\varphi\lambda_2}\right]\left[\sigma\left(1,a,b\right), \sigma\left(2,a,b\right)\right]^T.\end{aligned} \tag{8}$$

Accordingly, the product of the two matrix exponentials can be expressed as

$$\begin{aligned}\mathbf{N}\left(\varphi_1,\varphi_2\right) &= e^{\varphi_1\mathbf{A}_3 T_s/2\pi}e^{\varphi_2\mathbf{A}_1 T_s/2\pi}\\ &= \begin{bmatrix}\rho\left(\varphi_1,1,1\right) & \rho\left(\varphi_1,1,2\right)\\ \rho\left(\varphi_1,2,1\right) & \rho\left(\varphi_1,2,2\right)\end{bmatrix}\\ &\quad\times\begin{bmatrix}\rho\left(\varphi_2,1,1\right) & -\rho\left(\varphi_2,1,2\right)\\ -\rho\left(\varphi_2,2,1\right) & \rho\left(\varphi_2,2,2\right)\end{bmatrix}.\end{aligned} \tag{9}$$

By further analyzing the discrete-time iterative expressions (5) and (6), it can be concluded that the selection of the sampling moment of the state vector $\mathbf{x}_n$ has the significant influence on the complexity of the iterative expressions. Compared with the conventional discrete-time iteration [17], [32], the complexity of (5) and (6) will drastically decrease when the moment of the power switches S_5 and S_8 turning ON is selected as the sampling moment. The operating waveforms, in this case, are shown as Fig. 2. According to the decomposed matrix exponentials (7) and (8), the simplified coefficient matrices of the discrete-time

iterative model (5) can be expressed as

$$\begin{aligned}\boldsymbol{\Phi}_T &= \mathbf{N}(\pi,\pi)\\ \psi_T(\varphi_n) &= (\mathbf{N}(\pi,\pi) - 2\mathbf{N}(\pi,\varphi_n) + \mathbf{H}(\pi))\boldsymbol{\xi}_1\\ &\quad + (2\mathbf{H}(\varphi_n) - \mathbf{H}(\pi) - \mathbf{I})\boldsymbol{\xi}_2 \end{aligned} \tag{10}$$

where $\boldsymbol{\xi}_1 = \mathbf{A}_1^{-1}\mathbf{B}_1 V_1$, $\boldsymbol{\xi}_2 = \mathbf{A}_3^{-1}\mathbf{B}_1 V_1$.

Substituting the decomposed matrix exponentials into (10), the decomposed discrete-time model of the state variables can be obtained directly and analytically, as shown in (11). The state variables are also expressed separately instead of the vector form in (5). Therefore, the relationship among the state variables such as $i_{L(n+1)}$, v_C, and i_{Ln}, and the relationship among the circuit parameters and state variables can be analytically obtained. Accordingly, the decomposed discrete-time model will be applied to the multiscale oscillations analysis of the DAB converter for simplicity in the subsequent sections. The decomposed discrete-time iterative process is also feasible to be implemented in the digital controller

$$\begin{aligned} i_{L(n+1)} &= \mathbf{N}_{1,1} i_{Ln} + \mathbf{N}_{1,2} v_{Cn}\\ &\quad + \sum_{i=1}^{2} (\mathbf{N}_{1,i}(\pi,\pi) - 2\mathbf{N}_{1,i}(\pi,\varphi_n) + \mathbf{H}_{1,i}(\pi)A)\boldsymbol{\xi}_1(i)\\ &\quad + (2\mathbf{H}_{1,1}(\varphi_n) - \mathbf{H}_{1,1}(\pi) - 1)\boldsymbol{\xi}_2(1)\\ &\quad + (2\mathbf{H}_{1,2}(\varphi_n) - \mathbf{H}_{1,2}(\pi))\boldsymbol{\xi}_2(2)\\ v_{C(n+1)} &= \mathbf{N}_{2,1} i_{Ln} + \mathbf{N}_{2,2} v_{Cn}\\ &\quad + \sum_{i=1}^{2} (\mathbf{N}_{2,i}(\pi,\pi) - 2\mathbf{N}_{2,i}(\pi,\varphi_n) + \mathbf{H}_{2,i}(\pi))\boldsymbol{\xi}_1(i)\\ &\quad + (2\mathbf{H}_{2,1}(\varphi_n) - \mathbf{H}_{2,1}(\pi))\boldsymbol{\xi}_2(1)\\ &\quad + (2\mathbf{H}_{2,2}(\varphi_n) - \mathbf{H}_{2,2}(\pi) - 1)\boldsymbol{\xi}_2(2). \end{aligned} \tag{11}$$

2) Discrete-Time Modeling of the Digital Controller: In the previous works on the discrete-time modeling and the stability analysis of the DAB converter, the proportional control is always selected in the controller for simplicity. However, the proportional integral (PI) controller is widely utilized in the practical applications. The discrete-time models of the PI controller under the different conditions are obtained in this part. The ideal discrete-time model of the PI controller is shown as (12), where K_p and K_I are the proportional and integral constant, respectively.

$$\begin{aligned}\varphi(n) &= K_p e(n) + K_I \sum_{j=0}^{n} e(j)\\ \Delta\varphi(n) &= K_p \Delta e(n) + K_I e(n). \end{aligned} \tag{12}$$

The error value $e(n)$ is expressed as

$$\begin{aligned} e(n) &= V_{\mathrm{ref}n} - v_{2n}\\ &= V_{\mathrm{ref}n} - \mathbf{V}_{\mathrm{ex}}\mathbf{x}_n \end{aligned} \tag{13}$$

where $\mathbf{V}_{\mathrm{ex}} = [-R_o R_C/(R_o + R_C),\ R_o/(R_o + R_C)]$ represents the relationship between the output voltage and the state variables, which can be obtained according to the power circuit structure.

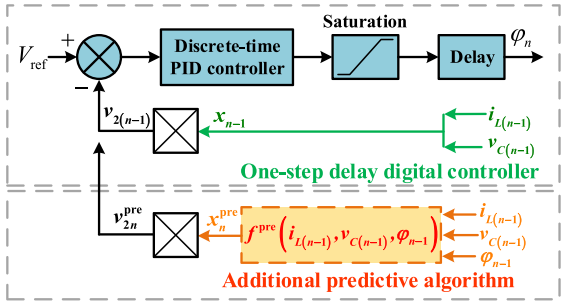

Fig. 4. Digital controller under the different control schemes.

However, the inherent control delay is inevitable in the digital controller. Therefore, the discrete-time iterative model of the PI controller [38] under the one-step control delay can be expressed as

$$\varphi(n) = K_p e(n-1) + K_I \sum_{j=0}^{n-1} e(j). \tag{14}$$

Accordingly, the discrete-time model of the incremental digital PI controller with the one-step digital control delay is expressed as

$$\begin{aligned}\varphi(n+1) &= \varphi(n) + \Delta\varphi(n)\\ \Delta\varphi(n) &= K_p \Delta e(n) + K_I e(n)\\ &= K_p(e(n) - e(n-1)) + K_I e(n)\\ &= k_1 e(n) + k_2 e(n-1) \end{aligned} \tag{15}$$

where $k_1 = K_p + K_I$, $k_2 = -K_p$, $K_I = K_p T_s/T_I$. T_s and T_I are the switching cycle and integral time constant, respectively.

The inherent one-step delay could deteriorate the system performance or even lead to the instability of the DAB converter in some cases. Fortunately, the decomposed discrete-time model of the DAB converter has a simple structure, which can be easily applied to the digital controller to compensate the control delay. The digital controller under the different control schemes is illustrated in Fig. 4. The additional predictive algorithm is shown as (16), where the predictive function f^{pre} is realized through the decomposed discrete-time iterative process of (11). It can also be found that the additional predictive algorithm is noninvasive, which can be easily implemented in the conventional one-step delay digital controller without changing any parts of the original controller to eliminate the effect of the digital control delay. Besides, compared with the methods in [17] and [33], the decomposed discrete-time iteration can be easily realized in the digital controller without affecting the calculation accuracy of the exponential matrices. In addition, the predictive algorithm still works when the more complicated modulation method is applied to the DAB converter [39] or some system parameters frequently change. Therefore, the proposed method also has the potential to be applied to other converters with the digital

control delay

$$\begin{aligned}\mathbf{x}_n^{\mathrm{pre}} &= f^{\mathrm{pre}}\left(i_{L(n-1)}, v_{C(n-1)}, \varphi_{n-1}\right)\\ &= \mathbf{\Phi}_T \mathbf{x}_{n-1} + \psi_T\left(\varphi_{n-1}\right).\end{aligned} \tag{16}$$

III. Multiscale Oscillations of the DAB Converter

A. Jacobian Matrix and Floquet Multipliers of the DAB Converter

The Jacobian matrix and Floquet multipliers are the effective tools to conduct the stability analysis of the DAB converter. In this part, the Jacobian matrices of the digitally controlled DAB converter under the different control schemes are analytically obtained according to the decomposed discrete-time model. The DAB converter system with the discrete-time digital PI controller under the one-step delay can be expressed as

$$\begin{cases} i_{\mathrm{L}(n+1)} = \begin{bmatrix}1\ 0\end{bmatrix}\mathbf{x}_{(n+1)} \\ v_{\mathrm{C}(n+1)} = \begin{bmatrix}0\ 1\end{bmatrix}\mathbf{x}_{(n+1)} \\ \varphi_{(n+1)} = \varphi_{(n)} + k_1\left(V_{\mathrm{ref}n} - \mathbf{V}_{\mathrm{ex}}\mathbf{x}_n\right) \\ \qquad\qquad + k_2\left(V_{\mathrm{ref}(n-1)} - \mathbf{V}_{\mathrm{ex}}\mathbf{x}_{(n-1)}\right) \\ \varphi_{(n+1)} \in [0, \pi/2]\ . \end{cases} \tag{17}$$

Since the phase shift angle $\varphi_{(n+1)}$ is related to the state variables in both the *n*th and (*n*-1)th switching cycles, the following formula transformation is utilized to rewrite the discrete-time system:

$$\begin{cases} y_{1n} = i_{L(n-1)} \\ y_{2n} = i_{Ln} \\ z_{1n} = v_{C(n-1)} \\ z_{2n} = v_{Cn}\ . \end{cases} \tag{18}$$

The standard form of the discrete-time iterative model of the DAB converter system is finally expressed as (19) when the formula transformation is applied to (17)

$$\begin{cases} y_{1(n+1)} = y_{2n} \\ y_{2(n+1)} = [1\ \ 0]\left(\mathbf{\Phi}_T\left(\varphi_n\right)\begin{bmatrix} y_{2n} \\ z_{2n}\end{bmatrix} + \psi_T\left(\varphi_n\right)\right) \\ z_{1(n+1)} = z_{2n} \\ z_{2(n+1)} = [0\ \ 1]\left(\mathbf{\Phi}_T\left(\varphi_n\right)\begin{bmatrix} y_{2n} \\ z_{2n}\end{bmatrix} + \psi_T\left(\varphi_n\right)\right) \\ \varphi_{(n+1)} = \varphi_{(n)} + k_1\left(V_{\mathrm{ref}n} - \mathbf{V}_{\mathrm{ex}}\begin{bmatrix} y_{2n} \\ z_{2n}\end{bmatrix}\right) \\ \qquad\qquad + k_2\left(V_{\mathrm{ref}(n-1)} - \mathbf{V}_{\mathrm{ex}}\begin{bmatrix} y_{1n} \\ z_{1n}\end{bmatrix}\right)\ . \end{cases} \tag{19}$$

According to the discrete-time iterative map of the state variables, the Jacobian matrix of the DAB converter system as shown in (20) can be calculated by taking the partial derivatives of (19) on the fixed point (X ϕ)

$$\mathbf{J} = \begin{bmatrix} \frac{\partial y_{1(n+1)}}{\partial y_{1n}} & \frac{\partial y_{1(n+1)}}{\partial z_{1n}} & \frac{\partial y_{1(n+1)}}{\partial y_{2n}} & \frac{\partial y_{1(n+1)}}{\partial z_{2n}} & \frac{\partial y_{1(n+1)}}{\partial \varphi_n} \\ \frac{\partial z_{1(n+1)}}{\partial y_{1n}} & \frac{\partial z_{1(n+1)}}{\partial z_{1n}} & \frac{\partial z_{1(n+1)}}{\partial y_{2n}} & \frac{\partial z_{1(n+1)}}{\partial z_{2n}} & \frac{\partial z_{1(n+1)}}{\partial \varphi_n} \\ \frac{\partial y_{2(n+1)}}{\partial y_{1n}} & \frac{\partial y_{2(n+1)}}{\partial z_{1n}} & \frac{\partial y_{2(n+1)}}{\partial y_{2n}} & \frac{\partial y_{2(n+1)}}{\partial z_{2n}} & \frac{\partial y_{2(n+1)}}{\partial \varphi_n} \\ \frac{\partial z_{2(n+1)}}{\partial y_{1n}} & \frac{\partial z_{2(n+1)}}{\partial z_{1n}} & \frac{\partial z_{2(n+1)}}{\partial y_{2n}} & \frac{\partial z_{2(n+1)}}{\partial z_{2n}} & \frac{\partial z_{2(n+1)}}{\partial \varphi_n} \\ \frac{\partial \varphi_{(n+1)}}{\partial y_{1n}} & \frac{\partial \varphi_{(n+1)}}{\partial z_{1n}} & \frac{\partial \varphi_{(n+1)}}{\partial y_{2n}} & \frac{\partial \varphi_{(n+1)}}{\partial z_{2n}} & \frac{\partial \varphi_{(n+1)}}{\partial \varphi_n} \end{bmatrix}\Bigg|_{(\mathrm{X},\,\phi)}. \tag{20}$$

Then the Floquet multipliers can be obtained by calculating the eigenvalues of the Jacobian matrix **J** through

$$\det\left(\lambda\mathbf{I} - \mathbf{J}\right) = 0 \tag{21}$$

where **I** is the identity matrix of the appropriate size.

1) Calculation of the Fixed Point: According to the symmetric characteristics of the state variables in the steady state as shown in Fig. 2, the state variables at the half a switching cycle can be derived as

$$\mathbf{x}_{n2} = \mathbf{I}_{\mathrm{HC}}\mathbf{x}_n \tag{22}$$

where

$$\mathbf{I}_{\mathrm{HC}} = \begin{bmatrix} -1 & 0 \\ 0 & 1 \end{bmatrix}.$$

Based on the discrete-time iteration of the state variables in Fig. 3, the relationship between $\mathbf{x}_n$ and $\mathbf{x}_{n2}$ can also be obtained in (23) according to the decomposed discrete-time iterative process

$$\begin{aligned}\mathbf{x}_{n2} &= f_{n2}\left(f_{n1}\left(\mathbf{x}_n, \varphi_n\right)\right)\\ &= \mathbf{H}'\left(\pi\right)\mathbf{x}_n + \left(\mathbf{H}'\left(\pi\right) - 2\mathbf{H}'\left(\varphi_n\right) + \mathbf{I}\right)\boldsymbol{\xi}_1\end{aligned} \tag{23}$$

where $\mathbf{H}'(\varphi_n) = e^{\varphi_n \mathbf{A}_1 T_s/2\pi}$.

Through the simultaneous formulas (22) and (23), the fixed point can be expressed as

$$\begin{aligned}\mathbf{X} &= \left(I_{\mathrm{L}}, V_{\mathrm{C}}\right)\\ &= \left(\mathbf{I}_{\mathrm{HC}} - \mathbf{H}'\left(\pi\right)\right)^{-1}\left(\mathbf{H}'\left(\pi\right) - 2\mathbf{H}'\left(\varphi_n\right) + \mathbf{I}\right)\boldsymbol{\xi}_1.\end{aligned} \tag{24}$$

Since the steady-state error of the DAB converter with PI controller is zero, the phase shift angle ϕ in the steady state can be calculated according to

$$V_{\mathrm{ref}} = \mathbf{V}_{ex}\mathbf{X}. \tag{25}$$

2) Jacobian Matrix of the DAB Converter Under One-Step Delay Control: According to the decomposed discrete-time model of the DAB converter, the elements of the Jacobian matrix can be easily obtained in the analytical form

$$\mathbf{P}=\frac{\partial \mathbf{x}_{n+1}}{\partial \mathbf{x}_n}=\mathbf{N}(\pi,\pi)$$
$$\mathbf{Q}=\frac{\partial \mathbf{x}_{n+1}}{\partial \varphi_n}=-\mathbf{N}(\pi,\varphi_n)T_s\mathbf{B}_1V_1-\mathbf{H}(\varphi_n)T_s\mathbf{B}_2V_1. \tag{26}$$

Let

$$[-k_2\mathbf{V}_{ex}\quad -k_1\mathbf{V}_{ex}]=[c_1\quad c_2\quad c_3\quad c_4],$$
$$\mathbf{P}=\begin{bmatrix}a_1 & a_2\\ a_3 & a_4\end{bmatrix},$$
$$\mathbf{Q}=\begin{bmatrix}b_1\\ b_2\end{bmatrix},$$

then the Jacobian matrix of the DAB converter under the one-step delay control is expressed as

$$\mathbf{J}_1=\begin{bmatrix}0 & 0 & 1 & 0 & 0\\ 0 & 0 & 0 & 1 & 0\\ 0 & 0 & a_1 & a_2 & b_1\\ 0 & 0 & a_3 & a_4 & b_2\\ c_1 & c_2 & c_3 & c_4 & 1\end{bmatrix}\Bigg|_{(\mathrm{X},\,\phi)}. \tag{27}$$

3) Jacobian Matrix of DAB Converter With the Predictive Control: The dual active bridge converter system with the additional predictive control algorithm is shown as (28). The discrete-time iterative relationship of the state variables in the power stage is the same as that with a one-step digital control delay. However, the discrete-time map of the state variables in the digital controller is quite different. The phase shift angle $\varphi_{(n+1)}$ is no longer related with the state variables in the (n-1)th switching cycle

$$\begin{cases} i_{L(n+1)}=[1\ \ 0]\left(\mathbf{\Phi}_T(\varphi_n)\begin{bmatrix}i_{Ln}\\ v_{Cn}\end{bmatrix}+\psi_T(\varphi_n)\right)\\ v_{C(n+1)}=[0\ \ 1]\left(\mathbf{\Phi}_T(\varphi_n)\begin{bmatrix}i_{Ln}\\ v_{Cn}\end{bmatrix}+\psi_T(\varphi_n)\right)\\ \varphi_{(n+1)}=\varphi_{(n)}+k_1\left(V_{\mathrm{ref}(n+1)}-\mathbf{V}_{\mathrm{ex}}\begin{bmatrix}i^{pre}_{L(n+1)}\\ v^{pre}_{C(n+1)}\end{bmatrix}\right)\\ \qquad\qquad +k_2\left(V_{\mathrm{ref}n}-\mathbf{V}_{\mathrm{ex}}\begin{bmatrix}i_{Ln}\\ v_{Cn}\end{bmatrix}\right). \end{cases} \tag{28}$$

Similarly, the Jacobian matrix of the DAB converter with the additional predictive algorithm can be easily obtained according to the decomposed discrete-time model. It is notable that the dimension of the Jacobian matrix as expressed in (29) is shown at bottom of the page has declined to three compared with that under the one-step delay control.

TABLE I
SPECIFICATIONS OF THE DAB CONVERTER PROTOTYPE

Symbol	Quantity	Values
V_1	Input voltage	72V
L	Sum of the external and leakage inductance	35.49μH
R_{eq}	Sum of the winding resistance and on-resistance of switching devices	0.38Ω
C_{o}	Output capacitor	500μF
R_{o}	Load resistance	10Ω
R_C	Equivalent series resistance of the output capacitor	0.05Ω
n	Turns ratio of the transformer	1
f_s	Switch frequency	20kHz
V_{ref}	Reference voltage	72V
K_p	Proportional constant	0.75
K_I	Integral constant	200

B. Multiscale Oscillations of the DAB Converter

In the practical applications, the digitally controlled DAB converter could encounter the different kinds of oscillations or even abruptly jump to the unstable state under some system parameters and working conditions, which could downgrade the system performance and have a damaging effect on the converter. The oscillation phenomena can mainly be summarized as the slow-scale low-frequency oscillation and the fast-scale subharmonic oscillation. According to the Jacobian matrices of the DAB converter under the different control schemes, the Floquet multipliers can be easily obtained via (21), which determines not only the stability of the system but also the oscillation type and the sudden jump phenomena.

There are four Floquet multipliers in the one-step delay controlled DAB converter with the parameters of Table I. The loci of the Floquet multipliers are illustrated in Fig. 5 with the variation of inductance L. The corresponding magnitude and phase of the Floquet multipliers are also shown in Fig. 6 when L varies from 34 to 59.03 μH. It can be found that there is a Floquet multiplier λ_4 almost remaining settled on the real axis within the unit circle. Besides, there is a conjugate pair of Floquet multipliers λ_1 and λ_2 moving from outside of the unit circle to the inside. Accordingly, the DAB converter will transit from the unstable state to the stable one. In addition, there exists a Floquet multiplier λ_3 moving along the real axis from the inside of the unit circle to the outside in the positive direction. Contrary to the conjugate Floquet multipliers crossing case, the DAB converter will jump from the stable state to the unstable one in this case.

$$\mathbf{J}_2=\begin{bmatrix}a_1 & a_2 & b_1\\ a_3 & a_4 & b_2\\ c_1+c_3a_1+c_4a_3 & c_2+c_3a_2+c_4a_4 & 1+c_3b_1+c_4b_2\end{bmatrix}\Bigg|_{(\mathrm{X},\,\phi)} \tag{29}$$

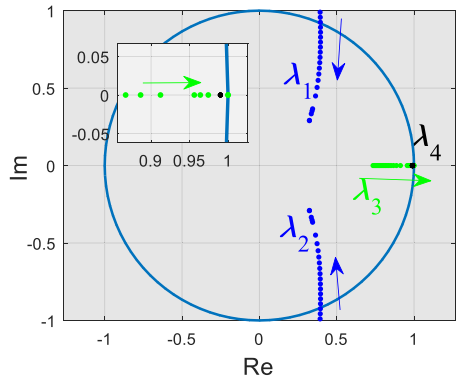

Fig. 5. Loci of the Floquet multipliers under the one-step delay control.

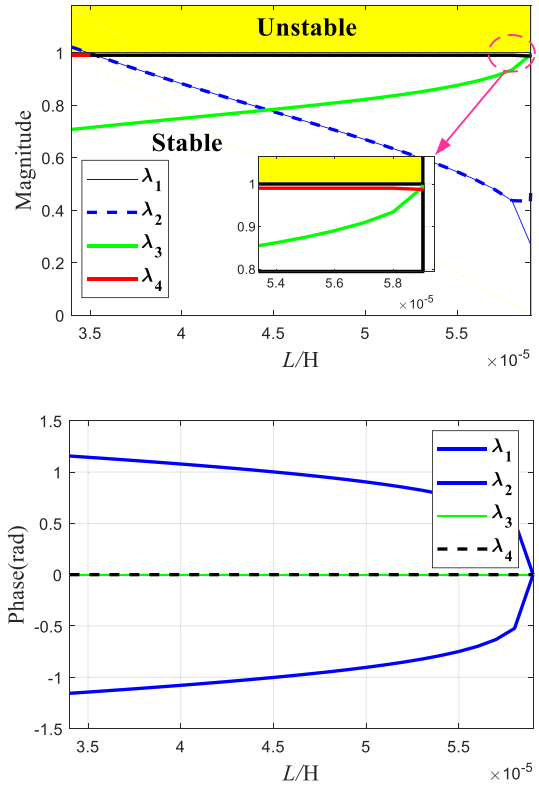

Fig. 6. Magnitude and phase of the Floquet multipliers under the one-step delay control.

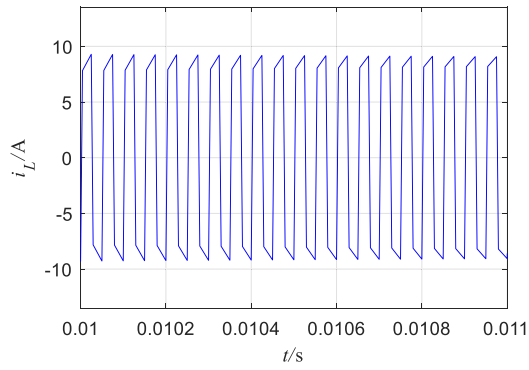

Fig. 7. Stable state inductor current waveform.

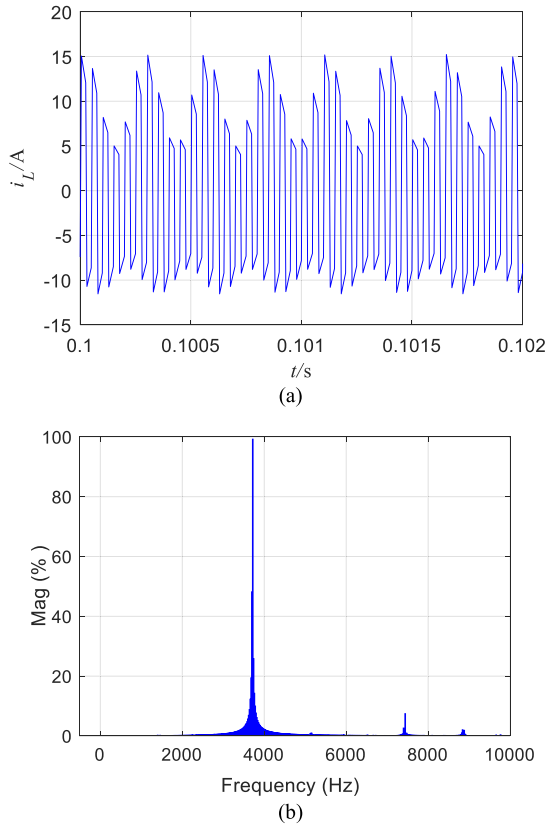

Fig. 8. Slow-scale low-frequency oscillation of the inductor current. (a) Inductor current waveform. (b) FFT of the inductor current.

The stable inductor current of the DAB converter with the parameters of Table I is shown in Fig. 7. According to the magnitude plot of the Floquet multipliers in Fig. 6, the conjugate pair of Floquet multipliers will locate on the unit circle when the inductance L decreases to about 34.7 μH. In this case, the Hopf bifurcation will occur in the DAB converter with a one-step digital control delay and the inductor current will exhibit the slow-scale low-frequency oscillation. The corresponding inductor current and its fast Fourier transformer (FFT) with the low-frequency oscillation are shown in Fig. 8. According to the FFT analysis result, the oscillation frequency of the inductor current in this case is about 3700 Hz, which corresponds to the frequency of the inductor current envelope. Compared with the stable state, the inductor current has a much higher amplitude and is not symmetric within a switching cycle, which could lead to the saturation of the transformer and increase the stress of other devices.

According to the magnitude plot of the Floquet multipliers in Fig. 6, the conjugate pair of Floquet multipliers will enter the interior of the unit circle when the inductance L continues to increase from 34 μH, whereas the Floquet multiplier λ_3 will move along the real axis in the positive direction. When the inductance L increases to 59.03 μH, λ_3 will reach the unit circle along the real axis. In this situation, the extremely small

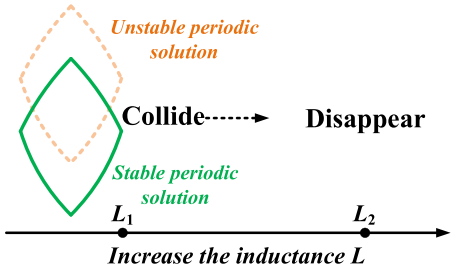

Fig. 9. Sudden jumps phenomena of the DAB converter.

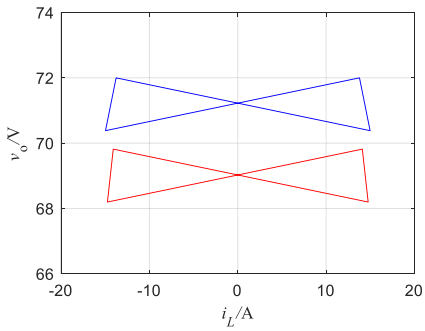

Fig. 10. Phase-plane waveform of the inductor current and output voltage.

disturbance on the inductance L could cause the DAB converter to suddenly jump to the unstable state, even though the system is supposed to have a large stability margin according to the conventional stability margin criteria [34]. As shown in Fig. 9, the stable periodic operation of the DAB converter could suddenly disappear when the inductance suffers from the extremely small disturbance from L_1 to L_2, which has been plaguing the engineers a lot. This phenomenon is actually caused by the collision of the stable periodic solution and the latent unstable periodic solution (The periodic solutions are on the phase plane where the inductor current i_L is the y-axis and the output voltage v_o is the z-axis). Accordingly, the stable periodic solution is suddenly annihilated and no normal periodic operation exists in the DAB converter [40], [41]. Finally, the DAB converter will switch from the normal periodic operation state to the state where the controller is saturated. As shown in Fig. 10, a tiny disturbance of the inductance L at the bifurcation point will cause the output voltage to jump from 72 V to about 69.5 V.

When the additional predictive algorithm is applied to the digitally controlled DAB converter with the parameters of Table I, there are three Floquet multipliers. The loci of the Floquet multipliers are illustrated in Fig. 11 when the inductance L varies from 23 to 59 μH. The corresponding magnitude and phase of the Floquet multipliers are also shown in Fig. 12. Similar to the DAB converter with the one-step delay, there also exists a Floquet multiplier λ_3 remaining settled on the real axis within the unit circle and a Floquet multiplier λ_2 moving along the real axis from the inside of the unit circle to the outside in the positive direction. Different from the conjugate pair of Floquet multipliers entering the interior of the unit circle from the outside in the one-step delay controlled DAB converter, there is only one Floquet multiplier λ_1 entering the unit circle along the real axis in the positive direction.

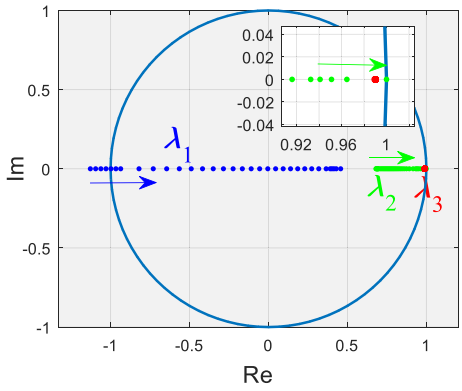

Fig. 11. Loci of the Floquet multipliers when the predictive algorithm is applied.

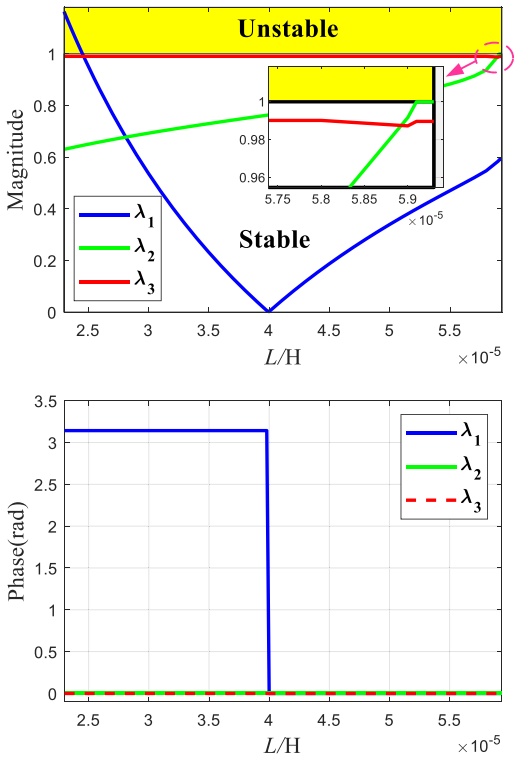

Fig. 12. Magnitude and phase of the Floquet multipliers with the predictive algorithm.

The stable intervals of system parameters expand when the additional predictive algorithm is applied to compensate the digital control delay. However, when inductance L is further decreased to 24.5 μH, the Floquet multiplier λ_1 will locate at the unit circle, which indicates the period-doubling bifurcation of the DAB converter. The inductor current will correspondingly exhibit the fast-scale subharmonic oscillation as shown in Fig. 13. In this case, the inductor current has the very high amplitude and large ripple. According to the FFT analysis, there exists a large spectral component at half the switching frequency, which indicates the subharmonic oscillation.

Besides, the DAB converter without digital control delay could also experience the sudden jump phenomena under some system parameters or working conditions. For example, when

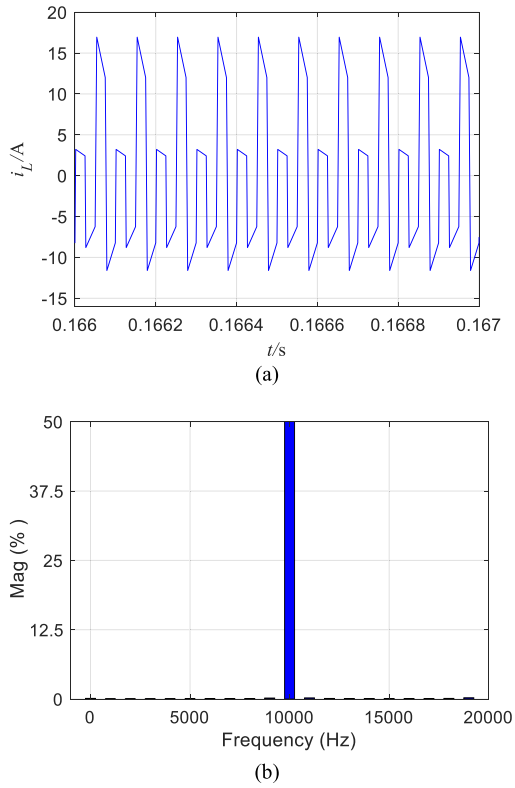

Fig. 13. Fast-scale subharmonic oscillation of the inductor current. (a) Inductor current waveform. (b) FFT of the inductor current.

the inductance L increases to about 59 μH, the normally operated DAB converter with the sufficient stability margin could suddenly jump to the unstable state under the slight disturbance on the inductance L.

It can be discovered that the sudden jump phenomena could occur in both the one-step delay controlled DAB converter and the DAB converter without digital control delay. However, the slow-scale low-frequency oscillation is prone to appear in the one-step delay controlled DAB converter, whereas the fast-scale subharmonic oscillation is limited to the DAB converter without digital control delay. The detailed analysis of the sudden jump phenomena and the multiscale oscillations of the DAB converter is carried out in the rest of the article.

IV. Multiscale Oscillations Analysis

Since the different characteristics of the Floquet multipliers determine the multiscale oscillations of the DAB converter, the analysis of the Jacobian matrix and Floquet multipliers is conducted from different perspectives in this section. The correlation factor of the discrete-time DAB converter system is first proposed to reveal which state variable has the significant influence on the Floquet multipliers that determine the multiscale oscillations. Accordingly, the Gershgorin bands analysis of the selected state variables is applied to reveal the influence of the digital control delay to the multiscale oscillations. In order to prevent the occurrence of the multiscale oscillations through the reasonable parameters design, the key system parameters to the system stability are selected through the sensitivity analysis. Finally, the criteria of all the possible unstable phenomena of the DAB converter are obtained to form the stable parameter space of the selected key parameters.

A. Correlation Factor

According to the multiscale oscillations phenomena of the DAB converter in Section III, it can be found that the different forms of the Floquet multipliers and their unique way of moving have the decisive influence on the dynamic features of the different state variables. In this part, the correlation factor of the discrete-time system is proposed to analyze the relevance between the different Floquet multipliers and the state variables.

If the small disturbance $\delta\mathbf{x}_0$ is applied to the fixed point $\mathbf{x}^*$ at the initial moment, the fixed point at the kth switching cycle will evolve as

$$\begin{aligned}\mathbf{x}_k &= \mathbf{x}^* + \delta\mathbf{x}_k \\ &= \mathbf{x}^* + \mathbf{J}(\mathbf{x}^*)^k\delta\mathbf{x}_0\end{aligned} \tag{30}$$

where $\mathbf{J}$ is the Jacobian matrix that is analytically expressed in (27) and (29) according to the decomposed discrete-time model.

The disturbance $\delta\mathbf{x}_0$ will evolve as (31) at the kth switching cycle. $\mathbf{D}$ is the diagonal matrix composed of all the Floquet multipliers. $\mathbf{U}$ and $\mathbf{V}^T$ are the matrices of the right and left eigenvectors of the Jacobian matrix $\mathbf{J}$, respectively. Besides, the matrices $\mathbf{U}$ and $\mathbf{V}^T$ have the relationship of (32)

$$\begin{aligned}\delta\mathbf{x}_k &= \mathbf{J}^k\delta\mathbf{x}_0 \\ &= \left(\mathbf{U}\mathbf{D}\mathbf{V}^T\right)^k\delta\mathbf{x}_0 \\ \mathbf{D} &= \operatorname{diag}\left(\lambda_1\ \lambda_1\ \cdots\ \lambda_N\right) \qquad (31) \\ \mathbf{V}^T &= \mathbf{U}^{-1}. \qquad (32)\end{aligned}$$

By performing the equivalent transformation of $\mathbf{X} = \mathbf{U}\mathbf{Y}$, the ith element of the state variable disturbances in the kth switching cycle with the initial disturbance vector $\mathbf{y}_0 = \mathbf{U}^{-1}\delta\mathbf{x}_0$ is expressed as

$$\delta\mathbf{x}_k^i = \sum_{j=1}^{N}\mathbf{U}_{ij}\mathbf{y}_0^j(\lambda_j)^k \tag{33}$$

where $\mathbf{y}_0^j$ is the jth element of $\mathbf{y}_0$.

Assume only the ith state variable is applied the initial unit disturbance, then $\mathbf{y}_0$ can be expressed as

$$\mathbf{y}_0 = \mathbf{V}^T\delta\mathbf{x}_0 = \begin{bmatrix}\left(\mathbf{V}^T\right)_{1i} \\ \vdots \\ \left(\mathbf{V}^T\right)_{Ni}\end{bmatrix}. \tag{34}$$

When the initial disturbance (34) is substituted in (33), the evolvement of the state variables disturbance is finally expressed

TABLE II
CORRELATION FACTOR $|\mathbf{P}_{ij}|$ WITHOUT CONTROL DELAY

	$\lvert P^{\lambda_i}_{i_L}\rvert$	$\lvert P^{\lambda_i}_{v_C}\rvert$	$\lvert P^{\lambda_i}_{\varphi}\rvert$
λ_1	0.0914	0.0034	0.9052
λ_2	0.9194	0.0128	0.0935
λ_3	0.0108	1.0094	0.0013

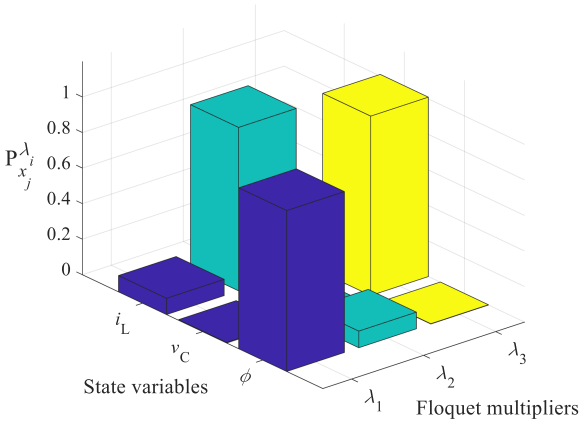

Fig. 14. Correlation factors between the state variables and Floquet multipliers without the digital control delay.

TABLE III
CORRELATION FACTOR $|\mathbf{P}_{ij}|$ WITH CONTROL DELAY

	$\lvert P^{\lambda_i}_{i_L(n)}\rvert$	$\lvert P^{\lambda_i}_{v_{C(n)}}\rvert$	$\lvert P^{\lambda_i}_{i_{L(n+1)}}\rvert$	$\lvert P^{\lambda_i}_{v_C(n+1)}\rvert$	$\lvert P^{\lambda_i}_{\varphi(n+1)}\rvert$
λ_1	0.1357	0.3847	0.1734	0.3965	0.5255
λ_2	0.1357	0.3847	0.1734	0.3965	0.5255
λ_3	0.3836	0.5639	0.6605	0.3939	0.1259
λ_4	0.0108	1.0217	0	0.0132	0.0023

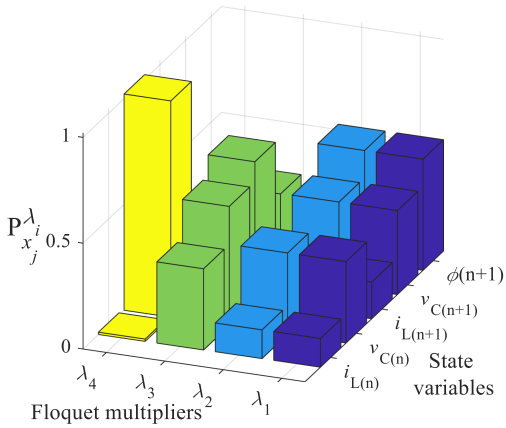

Fig. 15. Correlation factors between the state variables and Floquet multipliers with the digital control delay.

as

$$\delta \mathbf{x}_k^i = \sum_{j=1}^{N} \mathbf{U}_{ij}\left(\mathbf{V}^T\right)_{ji}(\lambda_j)^k = \sum_{j=1}^{N} \mathbf{U}_{ij}\mathbf{V}_{ij}(\lambda_j)^k. \tag{35}$$

Accordingly, the correlation factor $\mathbf{P}_{ij}$ of the discrete-time system is proposed as (36). The elements of the correlation factor matrix are the dimensionless quantities, which are irrelevant to the physical units of the state variables. The modulus of the correlation factor represents the relevant degree between the ith state variable and the jth Floquet multiplier

$$\mathbf{P}_{ij} = \mathbf{U}_{ij}\mathbf{V}_{ij}. \tag{36}$$

The correlation factors between the state variables and the Floquet multipliers of the DAB converter without digital control delay are shown in Table II. The Floquet multipliers λ_1, λ_2, and λ_3 are in accordance with those of Fig. 11. λ_1 is the Floquet multiplier that will lead to the fast-scale subharmonic oscillation of the system when crossing the unit circle along the negative direction of the real axis.

In order to intuitively represent the relationships between the state variables and the Floquet multipliers without the digital control delay, the correlation factors are illustrated in Fig. 14. It is obvious that each state variable corresponds to a Floquet multiplier with the close correlation. The fixed Floquet multiplier λ_3 is closely related to the dc voltage v_C. In addition, the inductor current i_L has the close relevance with the Floquet multiplier λ_2, which could lead to the sudden jump phenomena of the system. Besides, the phase shift angle φ is closely related to the Floquet multiplier λ_1, which could result in the subharmonic oscillation.

The correlation factors between the state variables and Floquet multipliers of the DAB converter with one-step digital control delay are shown in Table III and Fig. 15. The fixed Floquet multiplier λ_4 is still closely related to the dc voltage v_C. Similarly, the inductor current i_L has the close correlation with the Floquet multiplier λ_3, which could lead to the sudden jump phenomena of the system. Besides, the phase shift angle φ is closely related to the conjugate pair of Floquet multipliers λ_2 and λ_1, which could result in the slow-scale low-frequency oscillation. It is noticeable, however, the coupling between the state variables and the Floquet multipliers increases a lot compared with the correlation factors of Fig. 14 without the digital control delay.

B. Gershgorin Bands Analysis

According to the Floquet multipliers analysis, the conjugate pair of Floquet multipliers λ_1 and λ_2 are responsible for the slow-scale low-frequency oscillation in the DAB converter under the one-step delay control. Besides, the Floquet multiplier λ_1 in the DAB converter without digital control delay is responsible for the fast-scale subharmonic oscillation. It also indicates that these three Floquet multipliers have the close relationship with the phase shift angle φ according to the correlation factor analysis. In fact, the multiscale oscillations of the system are essentially the multiscale oscillations of the phase shift angle φ in the DAB converters under the SPS control. Therefore, the multiscale oscillations analysis of the DAB converter is also conducted in this part according to the Gershgorin bands analysis [42], [43] of the phase shift angle φ.

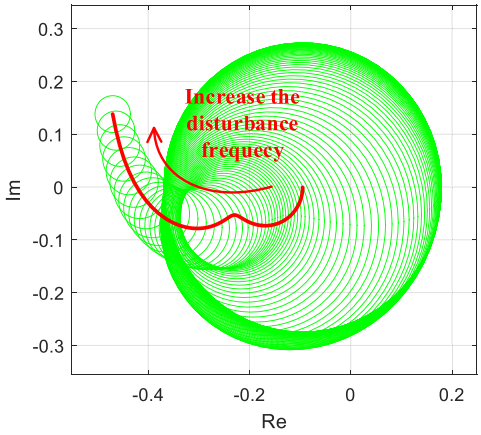

Fig. 16. Gershgorin bands of the phase shift angle φ_{n+1} in the DAB converter without digital control delay.

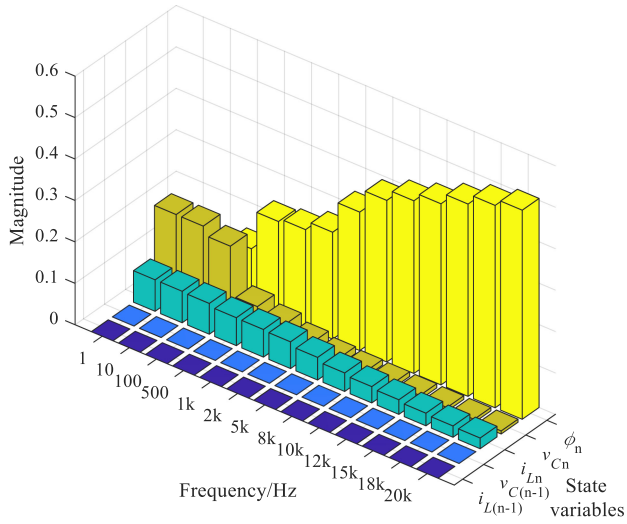

Fig. 17. Coupling of φ_{n+1} with other state variables in the DAB converter without digital control delay.

The discrete-time small-signal relationship of the state variables can be expressed as $\hat{\mathbf{x}}(n+1) = \mathbf{J} \cdot \hat{\mathbf{x}}(n)$ based on the Jacobian matrix $\mathbf{J}$. The Jacobian matrices under the different control schemes have been obtained in Section III according to the decomposed discrete-time model. The perturbations of the state variables at the different frequencies actually have the diverse influence on the state variables. The transfer function matrix of the system can be expressed as

$$\mathbf{W}(s) = \begin{bmatrix} \mathbf{W}_{11}(s) & \mathbf{W}_{12}(s) & \cdots & \mathbf{W}_{15}(s) \\ \mathbf{W}_{21}(s) & \mathbf{W}_{22}(s) & \cdots & \mathbf{W}_{25}(s) \\ \vdots & \vdots & & \vdots \\ \mathbf{W}_{51}(s) & \mathbf{W}_{52}(s) & \cdots & \mathbf{W}_{55}(s) \end{bmatrix} \tag{37}$$

where $\mathbf{W}_{ij}(s)$ represents the transfer function relationship between the *i*th state variable and the disturbance of the *j*th state variable at the different frequencies. Let $r_i = \sum_{\substack{j=1 \\ (j \neq i)}}^{5} |\mathrm{W}_{ij}|$ be the sum of the absolute values of the nondiagonal entries in the *i*th row. Then the circle centered at W_{ii} with radius r_i is called a Gershgorin circle. When the state variables of the DAB converter without digital control delay are, respectively, applied the unit disturbance with the frequency from 1 Hz to 20 kHz, the Gershgorin bands of the phase shift angle φ_{n+1} is shown in Fig. 16. Each Gershgorin circle corresponds to a certain disturbance frequency. It can be discovered from Fig. 16 that the Gershgorin circles gradually shrink and no longer contain the origin of the coordinates with the increase of the frequency. Therefore, the phase shift angle φ is gradually diagonally dominant and the coupling between φ_{n+1} and other state variables like v_{Cn}, i_{Ln}, $v_{C(n-1)}$, and $i_{L(n-1)}$ is gradually decreasing.

In order to evaluate the coupling characteristics of the state variables in the DAB converter without digital control delay, the magnitude of the coupling between φ_{n+1} and φ_n and other state variables under the different disturbance frequencies is shown in Fig. 17. It is obvious that φ_{n+1} is irrelevant with $v_{C(n-1)}$ and $i_{L(n-1)}$. Besides, φ_{n+1} has high degree of coupling with v_{Cn} in the frequency range less than 100 Hz. However, φ_{n+1} turns to have the close relationship with φ_n in the frequency range more than 1000 Hz, where the state variable v_C has the weak influence on the phase shift angle φ_{n+1}.

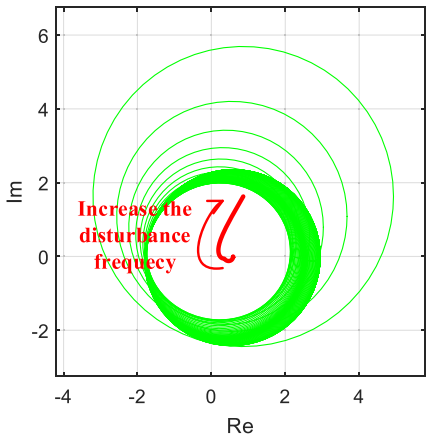

Fig. 18. Gershgorin bands of φ_{n+1} in the DAB converter with one-step digital control delay.

When the one-step delay exists in the digitally controlled DAB converter, the Gershgorin bands of φ_{n+1} are shown in Fig. 18. The radius of the Gershgorin circle does not change much with the slow-frequency state variable disturbances but increases significantly with the high-frequency disturbances, which is opposite to the DAB converter without digital control delay. Compared with the Gershgorin bands of φ_{n+1} in Fig. 16, the Gershgorin circles, in this case, have much larger radii and contain the origin of the coordinates, which indicate that φ_{n+1} of the DAB converter system with a one-step delay has the strong coupling with other state variables.

The detailed correlation of φ_{n+1} with φ_n and other state variables in the one-step delay controlled DAB converter is shown in Fig. 19. It is obvious that φ_{n+1} is still related with $v_{C(n-1)}$ and $i_{L(n-1)}$ because of the delay effect, which is different from Fig. 17 without the digital control delay. Besides, φ_{n+1}

TABLE IV
PARAMETER SENSITIVITY OF THE DAB CONVERTER WITH ONE-STEP DELAY

	$S_{R_C}^{\lambda_i}$	$S_{L}^{\lambda_i}$	$S_{R_o}^{\lambda_i}$	$S_{k_p}^{\lambda_i}$	$S_{k_I}^{\lambda_i}$	$S_{v_{ref}}^{\lambda_i}$	$S_{E}^{\lambda_i}$
λ_1	-0.055+0.199i	0.112-0.651i	0.002+0.011i	0.019+0.572i	0.004+0.003i	0.000+0.000i	0.050 + 0.253i
λ_2	-0.055-0.199i	0.112+0.651i	0.002-0.011i	0.019-0.572i	0.004-0.003i	0.000+0.000i	0.050 - 0.253i
λ_3	0.072+0.000i	0.108+0.000i	0.006+0.000i	-0.038+0.000i	0.001+0.000i	0.000+0.000i	-0.100 - 0.000i
λ_4	0.000-0.000i	-0.000-0.000i	-0.000-0.000i	-0.000-0.000i	-0.010-0.000i	0.000+0.000i	-0.000 + 0.000i

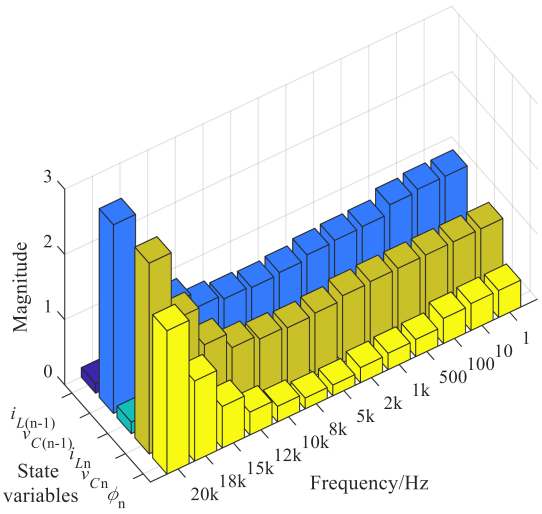

Fig. 19. Coupling of φ_{n+1} with other state variables in the DAB converter with one-step delay.

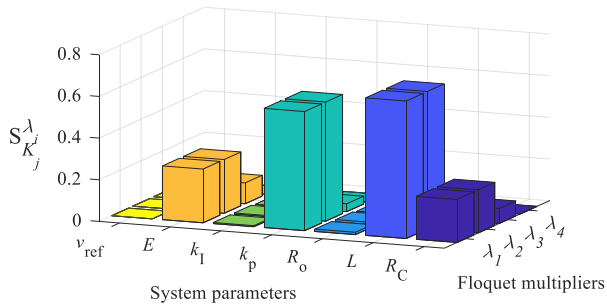

Fig. 20. Sensitivity of the Floquet multipliers under one-step delay.

is strongly coupled with the state variables v_{Cn} and $v_{C(n-1)}$ in the whole frequency range. Since the state variable v_C exhibits the low-frequency characteristics, the phase shift angle φ_{n+1} is prone to show the slow-scale low-frequency oscillation in the DAB converter with one-step delay. Whereas, φ_{n+1} of the DAB converter without digital control delay is diagonally dominant and has the weak coupling with v_C. Therefore, the DAB converter, in this case, is prone to exhibit the fast-scale subharmonic oscillation.

C. Sensitivity of the Floquet Multipliers

According to the loci analysis of the Floquet multipliers, the forms and moving features of the specific Floquet multipliers have the decisive influence on the multiscale oscillations and other unstable phenomena of the DAB converter. In order to prevent those phenomena by the reasonable parameters design, it is essential to analyze the relationship between the Floquet multipliers and the system parameters. Thus, the sensitivity analysis of Floquet multipliers to the system parameters of the DAB converter is proposed in this part.

The sensitivity of the Floquet multiplier λ_i to the system parameter K_j is expressed as (38), where $\mathbf{U}$ and $\mathbf{V}$ are the matrices of the right and left eigenvectors of the Jacobian matrix $\mathbf{J}$, respectively. Substituting the decomposed Jacobian matrices (27) and (29) into (38), the sensitivity of the Floquet multipliers to the system parameters can be easily obtained without calculating the Floquet multipliers in advance. Besides, the sensitivity of Floquet multipliers as shown in (38) is also dimensionless and irrelevant with the unit of the parameter K_j

$$S_{K_j}^{\lambda_i} = \frac{\partial \lambda_i}{\partial K_j} K_j = \frac{\mathbf{V}_i^T \left(\frac{\partial \mathbf{J}}{\partial K_j} \right) \mathbf{U}_i}{\mathbf{V}_i^T \mathbf{U}_i} K_j. \tag{38}$$

The parameter sensitivity of the Floquet multipliers in the one-step delay controlled DAB converter is shown in Table IV. The power stage parameters like the inductance L, load resistance R_o, input voltage E, equivalent series resistance R_C, and the digital controller parameters like the proportional constant k_p, integral constant k_I, and the output reference voltage v_{ref} are selected to conduct the sensitivity analysis. The sensitivity of the Floquet multipliers is also illustrated in Fig. 20, where the height of each bar represents the modulus of each element in Table IV. It can be intuitively discovered that the conjugate pair of Floquet multipliers λ_1, λ_2, and the real Floquet multiplier λ_3, which are related to the low-frequency oscillation and sudden jump phenomena, have high sensitivity to the system parameters L and k_p. It is also noticeable that the signs of the image parts of $S_L^{\lambda_1}$ and $S_L^{\lambda_2}$ are opposite to those of λ_1 and λ_2, respectively. However, the signs of the image parts of $S_{R_C}^{\lambda_1}$, $S_{R_C}^{\lambda_2}$, $S_{k_p}^{\lambda_1}$, and $S_{k_p}^{\lambda_2}$ are the same as those of λ_1 and λ_2, which indicates that λ_1 and λ_2 will gradually approach the unit circle with the increase of R_C and k_p and the system stability margin will accordingly shrink. Whereas, λ_1 and λ_2 will gradually move away from the

TABLE V
PARAMETER SENSITIVITY WITHOUT CONTROL DELAY

	$S^{\lambda_i}_{R_C}$	$S^{\lambda_i}_{L}$	$S^{\lambda_i}_{R_o}$	$S^{\lambda_i}_{k_p}$	$S^{\lambda_i}_{k_I}$	$S^{\lambda_i}_{v_{ref}}$	$S^{\lambda_i}_{E}$
λ_1	-0.660	2.179	0	-1.725	-0.008	0	-0.733
λ_2	0.070	0.104	0	-0.030	0.001	0	-0.093
λ_3	0	0	0	0	-0.010	0	0

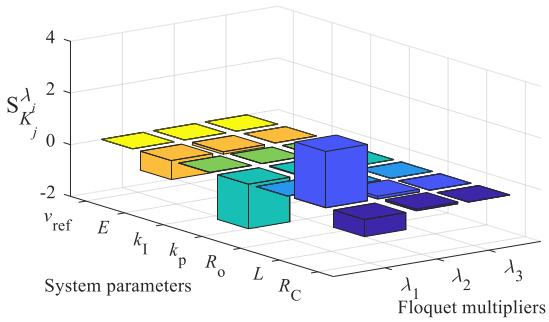

Fig. 21. Sensitivity of the Floquet multipliers without digital control delay.

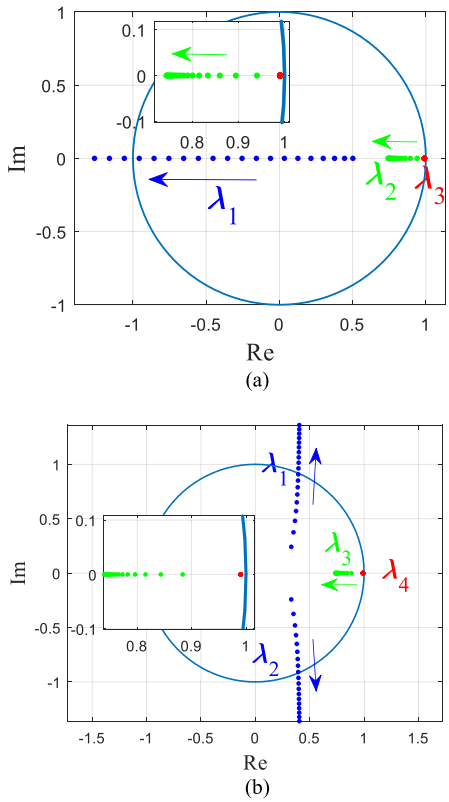

Fig. 22. Loci of the Floquet multipliers when *kp* varies from 0.5 to 1.5. (a) Without one-step delay. (b) With the one-step delay control.

unit circle with the increase of L and the system stability margin will accordingly expand.

When the additional predictive algorithm is applied to the DAB converter, the parameter sensitivity of the Floquet multipliers is shown in Table V. In this case, the Floquet multipliers λ_1 and λ_2 are related with the fast-scale subharmonic oscillation and the sudden jump phenomena, respectively. As illustrated in Fig. 21, the Floquet multipliers λ_1 and λ_2 still have the high sensitivity with the system parameters L, R_C, and k_p. The increase of L will also expand the stability margin, whereas the increase of R_C and k_p will decrease the stability margin.

Since the Floquet multipliers corresponding to the different unstable phenomena have high sensitivity to the system parameters like L, R_C and k_p, it is necessary to pay more attention to the design of these parameters. The loci of the Floquet multipliers when k_p varies from 0.5 to 1.5 are also shown in Fig. 22. It can be concluded that the loci of Floquet multipliers are similar to those when the inductance L varies as shown in Figs. 5 and 11. However, the direction of the loci, in this case, is the opposite of that when the inductance L varies, which verifies the conclusion above that the decisive Floquet multipliers to the multiscale oscillations of the DAB converter have the opposite sensitivity to the key system parameters k_p and L. Since the Floquet multipliers have quite low sensitivity to the integral constant k_I, the Floquet multipliers almost remain settled when k_I varies.

D. Parameter Spaces and Stability Boundaries

In this part, the parameter spaces and stability boundaries of the crucial system parameters L, R_C, and k_p are obtained according to the criteria of the multiscale oscillations in the digitally controlled DAB converter.

1) Stability Criteria of the DAB Converter With One-Step Delay Control: The Jacobian matrix $\mathbf{J}_1$ of the DAB converter with the one-step delay is obtained in (27) according to the decomposed discrete-time model. Then, the characteristic polynomial of $\mathbf{J}_1$ can be expressed as

$$\begin{aligned} f(\lambda) &= \det(\lambda\mathbf{I} - \mathbf{J}_1) \\ &= \lambda^4 + F_3\lambda^3 + F_2\lambda^2 + F_1\lambda + F_0 \end{aligned} \tag{39}$$

where

$$\begin{aligned} F_3 &= -1 - a_1 - a_4 \\ F_2 &= a_1 + a_4 + |\mathbf{P}| + k_2\mathbf{V}_{ex}\mathbf{Q} \\ F_1 &= -|\mathbf{P}| - k_2\mathbf{V}_{ex}\Upsilon + k_1\mathbf{V}_{ex}\mathbf{Q} \\ F_0 &= k_1\mathbf{V}_{ex}\Upsilon \\ \Upsilon &= \left[\, b_1a_4 - b_2a_2 \;\; b_2a_1 - b_1a_3 \,\right]^T. \end{aligned}$$

It is obvious the DAB converter with the one-step delay is a fourth-order system according to the characteristic polynomial of (39). Then, the Jury stability criterion can be applied to obtain the stability constraints of the fourth-order system. The characteristic polynomial coefficients yielding to (40) will guarantee

the stable operation of the DAB converter

$$\begin{cases} |F_0F_3 - F_1| < 1 - F_0^2 \\ |F_0| < 1 \\ (F_0-1)^2(F_0 - F_2 + 1) - (F_3 - F_1)(F_3F_0 - F_1) > 0 \\ f(1) > 0,\ f(-1) > 0\,. \end{cases} \tag{40}$$

Actually, the parameters satisfying $f(1) = F_3 + F_2 + F_1 + F_0 + 1 = 0$ correspond to the parameter boundary of the jump phenomena in the DAB converter. The equation $f(-1) = -F_3 + F_2 - F_1 + F_0 + 1 = 0$ constrains the parameter boundary of the fast-scale subharmonic oscillation phenomena. Besides, the parameters satisfying the equation $(F_0 - 1)^2(F_0 - F_2 + 1) - (F_3 - F_1)(F_3F_0 - F_1) = 0$ form the parameter boundary of the slow-scale low-frequency oscillation phenomena. It can also be discovered that the system parameters of the DAB converter with the one-step delay will not satisfy the equation $f(-1) = -F_3 + F_2 - F_1 + F_0 + 1 = 0$. In other words, the subharmonic oscillation actually does not exist in the DAB converter with the one-step digital control delay, which is consistent with the analysis of the previous parts.

As shown in Fig. 5, there exists a conjugate pair of Floquet multipliers $\lambda = a \pm b\mathrm{i}$ crossing the unit circle when the low-frequency oscillation appears. The corresponding oscillation frequency can be analytically expressed as

$$f_{\mathrm{osc}} = f_{\mathrm{s}} \times \left(\arctan\left|\frac{b}{a}\right|\right) \times \frac{1}{2\pi} \tag{41}$$

where $a = \frac{F_3 - F_1}{2F_0 - 2}$, $b = \sqrt{1 - a^2}$. The analyzed oscillation frequency is in accordance with the simulation results of Fig. 8 when the system parameters of Table I are substituted into the expression of analytical oscillation frequency.

2) Stability Criteria of the DAB Converter With the Additional Predictive Algorithm: When the proposed additional predictive algorithm based on the decomposed discrete-time model is applied to the DAB converter, the characteristic polynomial of the Jacobian matrix $\mathbf{J}_2$, as shown in (29), can be expressed as

$$\begin{aligned} f(\lambda) &= \det(\lambda\mathbf{I} - \mathbf{J}_2) \\ &= \lambda^3 + F'_2\lambda^2 + F'_1\lambda + F'_0 \end{aligned} \tag{42}$$

where

$$\begin{aligned} F'_2 &= -1 - a_1 - a_4 + k_2\mathbf{V}_{ex}\mathbf{Q} \\ F'_1 &= a_1 + a_4 + |\mathbf{P}| + k_1\mathbf{V}_{ex}\mathbf{Q} - k_2\mathbf{V}_{ex}\Upsilon \\ F'_0 &= -|\mathbf{P}| + k_1\mathbf{V}_{ex}\Upsilon. \end{aligned}$$

According to the characteristic polynomial of (42), the DAB converter without digital control delay changes into a third-order system. Similarly, the Jury stability criterion will be applied to obtain the stability constraints of the system. Therefore, the DAB converter will work in the stable state when the characteristic polynomial coefficients yield to the following constraints:

$$\begin{cases} |F'_0| < 1 \\ F'^2_0 - 1 < F'_0F'_2 - F'_1 \\ F'_0 + F'_1 + F'_2 + 1 > 0 \\ F'_0 - F'_1 + F'_2 - 1 < 0\,. \end{cases} \tag{43}$$

In this case, the equation $F'_0 - F'_1 + F'_2 - 1 = 0$ constrains the parameter boundary of the fast-scale subharmonic oscillation of the DAB converter. Besides, the system parameters satisfying $F'_0 + F'_1 + F'_2 + 1 = 0$ correspond to the sudden jump phenomena. In addition, the equation $F'^2_0 - F'_0F'_2 + F'_1 = 1$ constrains the parameter boundary of the low-frequency oscillation phenomena. Similarly, the system parameters will not satisfy the criterion of the slow-scale low-frequency oscillation phenomena in the DAB converter without digital control delay, which validates the analysis of the previous parts again.

3) Parameter Spaces and Stability Boundaries: According to the sensitivity analysis of the Floquet multipliers, the inductance L, equivalent series resistance R_C of the output capacitor and the proportional constant k_p of the controller have the significant influence on the system stability. Therefore, the parameter spaces about these system parameters can be obtained based on the proposed stability criteria of the different kinds of unstable phenomena. The detailed parameter spaces are illustrated in Fig. 23. Besides, the stability boundaries with the 50° phase margin are also obtained according to the conventional stability margin criterion [34], [35]. Both the stability boundaries and the boundaries with the 50° phase margin constraint expand significantly when the proposed additional predictive algorithm is applied. It is noticeable that there is 50° phase margin and the magnitude margin is actually also very large when the inductance L is about 49 μH according to the conventional stability margin criteria. However, in the practical operations, the sudden jump phenomena will occur in the DAB converter with this parameter and the system will jump from the stable operation to the undesired unstable state. Therefore, the parameters design according to the conventional stability margin criteria is not quite suitable for the DAB converter and cannot guarantee the stable operation of the system with sufficient stability margin. Whereas, the parameters design in this article will consider the criteria of all the possible unstable phenomena in the DAB converter. Therefore, the parameter spaces obtained are more comprehensive and reliable, which can provide the guidance for the practical parameters design.

V. Experimental Verification

In order to validate the theoretical analysis and the simulation results presented in the previous sections, an experimental prototype was built according to the specifications of Table I. The prototype of the digitally controlled DAB converter is depicted in Fig. 24. Each H-bridge consists of four IPP110N20N3G power-transistors from Infineon, rated at 88 A, 200 V. The power-transistors are driven by the circuit boards, which are composed of the 1ED020I12-F insulated-gate bipolar transistor (IGBT) driver integrated circuits (ICs) and other isolation and

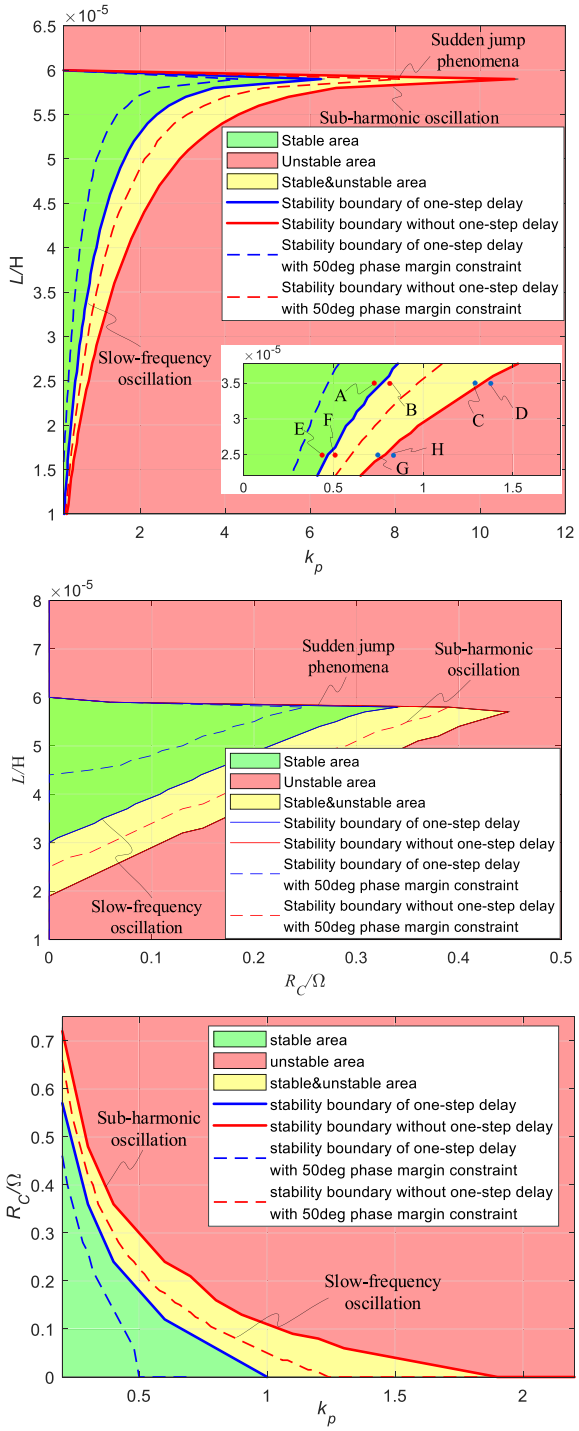

Fig. 23. Parameter spaces and the stability boundaries.

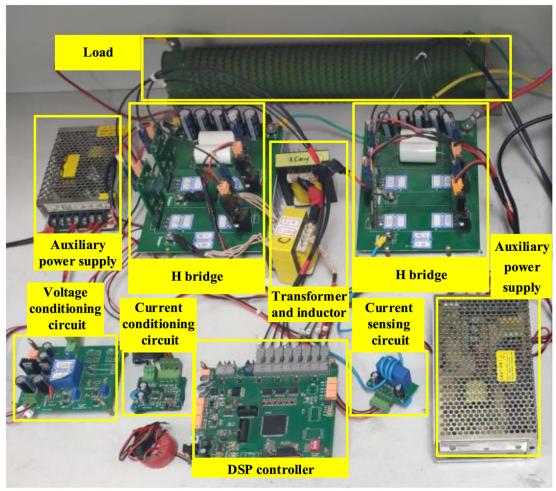

Fig. 24. Experimental prototype of the DAB converter.

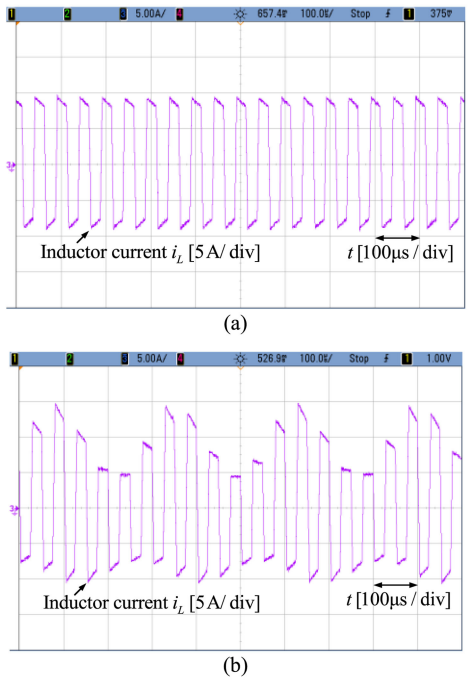

Fig. 25. Inductor current of the DAB converter with one-step delay. (a) $k_p = 0.77$ (b) $k_p = 0.78$.

amplifier parts. The high-frequency transformer is made up of the magnetic wires and the ferrite core from Ferroxcube. Besides, the auxiliary inductor is connected in series with one end of the transformer. The output voltage signal will be transmitted to the ADC module of the TMS320F28335 digital signal processor (DSP) controller through the voltage conditioning circuit, which contains the LV28-P voltage transducer and the TL082 operational amplifier. The inductor current signal will also be sent to the ADC module of the DSP controller through the current sensing and conditioning circuits, which contain the LA100-P/SA50 current transducer and the TL074 operational amplifiers. With the sampled inductor current and output voltage signals, the phase shift angle of the next switching cycle can be calculated in the digital controller according to the proposed algorithm.

The inductor current waveforms of the DAB converter with the one-step digital control delay are shown in Fig. 25. It can be observed that the converter is stable when the proportional constant k_p is 0.77, which corresponds to point A of the parameter space as shown in Fig. 23. However, the inductor current will exhibit the slow-scale low-frequency oscillation with the high

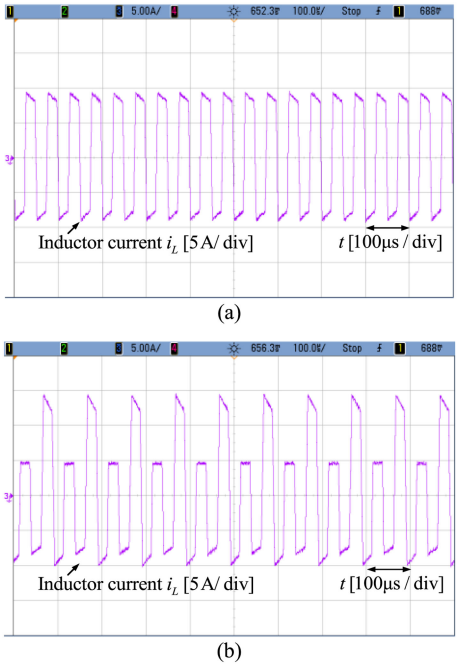

Fig. 26. Inductor current of the DAB converter without digital control delay. (a) $k_p = 1.36$ (b) $k_p = 1.37$.

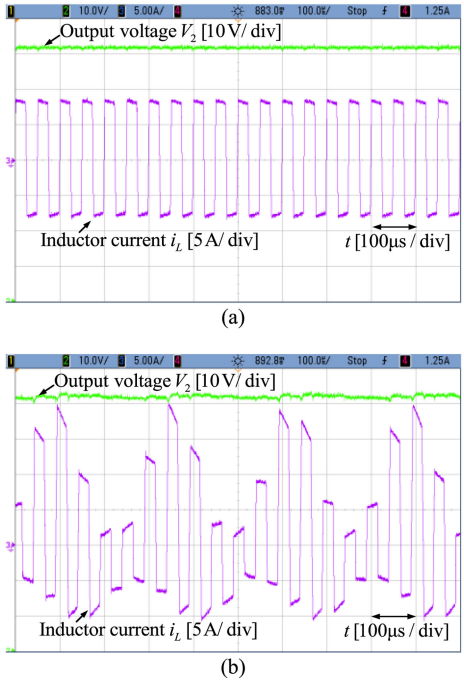

Fig. 27. Inductor current and output voltage of the DAB converter with one-step delay when L is 24.9 μH. (a) $k_p = 0.46$. (b) $k_p = 0.47$.

amplitude components when k_p increases to 0.78, which corresponds to the point B of the parameter space. When the proposed additional predictive algorithm is applied to compensate the digital control delay, the stable parameter intervals will expand a lot and the system is still stable when k_p increases to 1.36. However, the DAB converter will also enter the unstable state when continuing to increase k_p to about 1.37 and the inductor current will exhibit the fast-scale subharmonic oscillation with high amplitude. The inductor current waveforms of the DAB converter without digital control delay are shown in Fig. 26, which correspond to point C and D of the parameter space, respectively.

If the inductance L is decreased to 24.9 μH, the inductor current and output voltage waveforms of the DAB converter with one-step digital control delay are shown in Fig. 27. The system is stable when k_p is 0.46 and the slow-scale low-frequency oscillation will occur when k_p changes to 0.47, which correspond to point E and F of the parameter space, respectively. Besides, the inductor current and output voltage of the DAB converter without digital control delay are shown in Fig. 28. When k_p increases from 0.77 to 0.78, the system will transform from the stable state to the subharmonic oscillation, which corresponds to the point G and H of the parameter space, respectively. In addition, the inductor current amplitudes of Figs. 27(b) and 28(b) are much higher than those when the inductance L is 35.49 μH.

It can be observed that the ripple of the inductor current and output voltage will dramatically increase when the multiscale oscillations occur in the DAB converter, which has the jeopardizing effects on the performance of the system. Besides, the oscillation of the inductor current is particularly significant. The inductor current with the slow-scale oscillation contains a lot of undesirable low-frequency harmonic components. Whereas,

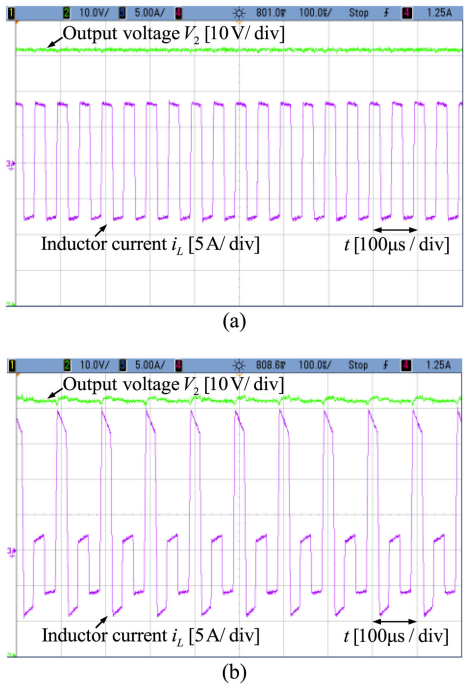

Fig. 28. Inductor current and output voltage of the DAB converter without digital control delay when L is 24.9 μH. (a) $k_p = 0.77$. (b) $k_p = 0.78$.

the harmonic of half the switching frequency becomes the main component of the current spectrum when the fast-scale subharmonic oscillation occurs. These harmonic components could cause the undesirable noise. In addition, the inductor current under these two kinds of oscillations has the characteristics of high amplitude and asymmetry. The asymmetrical inductor current will lead to a dc bias and generate the flux bias in the

transformer. The accumulation of the biased magnetic flux will eventually result in the transformer saturation and the sharp increase of the current flow, which could increase the device stress or destruct the power switches.

VI. Conclusion

In this article, the multiscale oscillations of the DAB converter are systematically analyzed based on the proposed decomposed discrete-time model. The decomposed discrete-time model has significantly simplified the conventional discrete-time model without reducing the calculation accuracy. Accordingly, the decomposed discrete-time model is applied to the controller design to eliminate the digital control delay. It also indicates that the characteristics of the multiscale oscillations in the DAB converter are determined by the forms and moving features of the Floquet multipliers. Therefore, the relationships among the state variables, system parameters and the Floquet multipliers are analytically investigated according to the proposed discrete-time correlation factor, sensitivity analysis, and the Gershgorin bands analysis of the DAB converter. Finally, the stability criteria of all the three kinds of unstable phenomena of the DAB converter are obtained, which are utilized to get the stability boundaries of the system parameters. It is also shown that the conventional margin criteria cannot guarantee the sufficient stability margin. Whereas, the parameter spaces obtained in this article consider all the possible unstable phenomena of the DAB converter and therefore is more reliable in the practical parameters design. The experimental results are also shown to be consistent with the simulation and theoretical analysis.

References

[1] B. Zhao, Q. Song, W. H. Liu, and Y. D. Sun, "Overview of dual-active-bridge isolated bidirectional DC-DC converter for high-frequency-link power-conversion system," *IEEE Trans. Power Electron.*, vol. 29, no. 8, pp. 4091–4106, Aug. 2014.

[2] D. Aggeler, J. Biela, S. Inoue, H. Akagi, and J. W. Kolar, "Bi-directional isolated dc-dc converter for next-generation power distribution-comparison of converters using Si and SiC devices," in *Proc. Power Convers. Conf.*, 2007, pp. 510–517.

[3] M. Ryu, H. Kim, J. Baek, H. Kim, and J. Jung, "Effective test bed of 380-V DC distribution system using isolated power converters," *IEEE Trans. Ind. Electron.*, vol. 62, no. 7, pp. 4525–4536, Jul. 2015.

[4] G. Ortiz, J. Biela, D. Bortis, and J. W. Kolar, "1 Megawatt, 20 kHz, isolated, bidirectional 12 kV to 1.2 kV DC-DC converter for renewable energy applications," in *Proc. Int. Power Electron. Conf.*, 2010, pp. 3212–3219.

[5] F. Xue, R. Yu, and A. Q. Huang, "A 98.3% efficient GaN isolated bidirectional DC–DC converter for DC microgrid energy storage system applications," *IEEE Trans. Ind. Electron.*, vol. 64, no. 11, pp. 9094–9103, Nov. 2017.

[6] H. Zhou, T. Bhattacharya, D. Tran, T. S. T. Siew, and A. M. Khambadkone, "Composite energy storage system involving battery and ultracapacitor with dynamic energy management in microgrid applications," *IEEE Trans. Power Electron.*, vol. 26, no. 3, pp. 923–930, Mar. 2011.

[7] Y. Jiang, L. Wang, Y. Wang, J. Liu, M. Wu, and G. Ning, "Analysis, design, and implementation of WPT system for EV's battery charging based on optimal operation frequency range," *IEEE Trans. Power Electron.*, vol. 34, no. 7, pp. 6890–6905, Jul. 2019.

[8] J. Shi, W. Gou, H. Yuan, T. Zhao, and A. Q. Huang, "Research on voltage and power balance control for cascaded modular solid-state transformer," *IEEE Trans. Power Electron.*, vol. 26, no. 4, pp. 1154–1166, Apr. 2011.

[9] T. Zhao, G. Wang, S. Bhattacharya, and A. Q. Huang, "Voltage and power balance control for a cascaded H-bridge converter-based solid-state transformer," *IEEE Trans. Power Electron.*, vol. 28, no. 4, pp. 1523–1532, Apr. 2013.

[10] H. Sangtaek and D. Divan, "Bi-directional DC/DC converters for plug-in hybrid electric vehicle (PHEV) applications," in *Proc. 23rd Annu. IEEE Appl. Power Electron. Conf. Expo.*, Feb. 2008, pp. 784–789.

[11] L. Xue, Z. Shen, D. Boroyevich, P. Mattavelli, and D. Diaz, "Dual active bridge-based battery charger for plug-in hybrid electric vehicle with charging current containing low frequency ripple," *IEEE Trans. Power Electron.*, vol. 30, no. 12, pp. 7299–7307, Dec. 2015.

[12] Y. Jiang, L. Wang, Y. Wang, J. Liu, X. Li, and G. Ning, "Analysis, design, and implementation of accurate ZVS angle control for EV battery charging in wireless high-power transfer," *IEEE Trans. Ind. Electron.*, vol. 66, no. 5, pp. 4075–4085, May 2019.

[13] Y. Jiang *et al.*, "Phase-locked loop combined with chained trigger mode used for impedance matching in wireless high power transfer," *IEEE Trans. Power Electron*., vol. 35, no. 4, pp. 4272–4285, Apr. 2020,.

[14] R. Morrison and M. G. Egan, "A new power-factor-corrected single-transformer UPS design," *IEEE Trans. Ind Appl.*, vol. 36, no. 1, pp. 171–179, Jan./Feb. 2000.

[15] A. El Aroudi, D. Giaouris, H. H.-C. Iu, and I. A. Hiskens, "A review on stability analysis methods for switching mode power converters," *IEEE J. Emerging Sel. Topics Circuits Syst.*, vol. 5, no. 3, pp. 302–315, Sep. 2015.

[16] F. Krismer and J. W. Kolar, "Accurate small-signal model for the digital control of an automotive bidirectional dual active bridge," *IEEE Trans. Power Electron.*, vol. 24, no. 12, pp. 2756–2768, Dec. 2009.

[17] L. Shi, W. Lei, Z. Li, J. Huang, Y. Cui, and Y. Wang, "Bilinear discrete-time modeling and stability analysis of the digitally controlled dual active bridge converter," *IEEE Trans. Power Electron.*, vol. 32, no. 11, pp. 8787–8799, Nov. 2017.

[18] S. P. Engel, N. Soltau, H. Stagge, and R. W. D. Doncker, "Dynamic and balanced control of three-phase high-power dual-active bridge DC–DC converters in DC-grid applications," *IEEE Trans. Power Electron.*, vol. 28, no. 4, pp. 1880–1889, Apr. 2013.

[19] H. Krishnamurthy and R. Ayyanar, "Stability analysis of cascaded converters for bidirectional power flow applications," in *Proc. IEEE 30th Int. Telecommun. Energy Conf.*, Sep. 2008, pp. 1–8.

[20] R. D. Middlebrook and S. Cuk, "A general unified approach to modelling switching-converter power stages," in *Proc. IEEE Power Electron. Specialists Conf.*, 1976, pp. 18–34.

[21] A. Forsyth and S. V. Mollov, "Modelling and control of DC-DC converters," *Power Eng. J.*, vol. 12, no. 5, pp. 229–236, Oct. 1998.

[22] H. Qin and J. W. Kimball, "Generalized average modeling of dual active bridge DC–DC converter," *IEEE Trans. Power Electron.*, vol. 27, no. 4, pp. 2078–2084, Apr. 2012.

[23] B. Hua, M. Chunting, W. Chongwu, and S. Gargies, "The dynamic model and hybrid phase-shift control of a dual-active-bridge converter," in *Proc. 34th Annu. Conf. IEEE Ind. Electron.*, Nov. 2008, pp. 2840–2845.

[24] H. Bai, Z. Nie, and C. C. Mi, "Experimental comparison of traditional phase-shift, dual-phase-shift, and model-based control of isolated bidirectional DC–DC converters," *IEEE Trans. Power Electron.*, vol. 25, no. 6, pp. 1444–1449, Jun. 2010.

[25] J. Guacaneme, G. Garcerá, E. Figueres, I. Patrao, and R. González-Medina, "Dynamic modeling of a dual active bridge DC to DC converter with average current control and load-current feed-forward," *Int. J. Circuit Theory Appl.*, vol. 43, no. 10, pp. 1311–1332, 2015, doi: 10.1002/cta.2012.

[26] K. Zhang, Z. Shan, and J. Jatskevich, "Large- and small-signal average-value modeling of dual-active-bridge DC–DC converter considering power losses," *IEEE Trans. Power Electron.*, vol. 32, no. 3, pp. 1964–1974, Mar. 2017.

[27] D. Maksimovic and R. Zane, "Small-signal discrete-time modeling of digitally controlled PWM converters," *IEEE Trans. Power Electron.*, vol. 22, no. 6, pp. 2552–2556, Nov. 2007.

[28] D. Costinett, R. Zane, and D. Maksimović, "Discrete-time small-signal modeling of a 1 MHz efficiency-optimized dual active bridge converter with varying load," in *Proc. IEEE 13th Workshop Control Modeling Power Electron.*, Jun. 2012, pp. 1–7.

[29] C. Zhao, S. D. Round, and J. W. Kolar, "Full-order averaging modelling of zero-voltage-switching phase-shift bidirectional DC-DC converters," *IET Power Electron.*, vol. 3, no. 3, pp. 400–410, 2010.

[30] D. Costinett, R. Zane, and D. Maksimovic, "Discrete time modeling of output disturbances in the dual active bridge converter," in *Proc. IEEE Appl. Power Electron. Conf. Expo.*, 2014, pp. 1171–1177.

[31] D. Costinett, "Reduced order discrete time modeling of ZVS transition dynamics in the dual active bridge converter," in *Proc. IEEE Appl. Power Electron. Conf. Expo.*, 2015, pp. 365–370.

[32] S. Ling, L. Wanjun, H. Jun, L. Zhuoqiang, C. Yao, and W. Yue, "Full discrete-time modeling and stability analysis of the digital controlled dual active bridge converter," in *Proc. IEEE 8th Int. Power Electron. Motion Control Conf.*, May 2016, pp. 3813–3817.
[33] V. Rajasekaran, S. Jian, and B. S. Heck, "Bilinear discrete-time modeling for enhanced stability prediction and digital control design," *IEEE Trans. Power Electron.*, vol. 18, no. 1, pp. 381–389, Jan. 2003.
[34] A. Riccobono and E. Santi, "Comprehensive review of stability criteria for DC power distribution systems," *IEEE Trans. Ind Appl.*, vol. 50, no. 5, pp. 3525–3535, Oct. 2014.
[35] J. Morroni, R. Zane, and D. Maksimovic, "Design and implementation of an adaptive tuning system based on desired phase margin for digitally controlled DC–DC converters," *IEEE Trans. Power Electron.*, vol. 24, no. 2, pp. 559–564, Feb. 2009.
[36] H. Bai, Z. Zhao, and C. Mi, "Framework and research methodology of short-timescale pulsed power phenomena in high-voltage and high-power converters," *IEEE Trans. Ind. Electron.*, vol. 56, no. 3, pp. 805–816, Mar. 2009.
[37] B. Hua, C. C. Mi, and S. Gargies, "The short-time-scale transient processes in high-voltage and high-power isolated bidirectional DC–DC converters," *IEEE Trans. Power Electron.*, vol. 23, no. 6, pp. 2648–2656, Nov. 2008.
[38] L. Zhao, H. Li, Y. Liu, and Z. Li, "High efficiency variable-frequency full-bridge converter with a load adaptive control method based on the loss model," *Energies*, vol. 8, no. 4, pp. 2647–2673, 2015.
[39] Y. Minami, N. Iijima, H. Mitsui, Y. Yoshida, and M. Sone, "High speed calculation of eigenvalue by digital signal processor," in *Proc. 35th Midwest Symp. Circuits Syst.*, 1992, pp. 1136–1139.
[40] M. di Bernardo, F. Garefalo, L. Glielmo, and F. Vasca, "Switchings, bifurcations, and chaos in DC/DC converters," *IEEE Trans. Circuits Syst. I, Fundam. Theory Appl.*, vol. 45, no. 2, pp. 133–141, Feb. 1998.
[41] C.-C. Fang, "Saddle-node bifurcation in the buck converter with constant current load," *Nonlinear Dyn.*, vol. 69, no. 4, pp. 1739–1750, 2012.
[42] J. D. Dasika, B. Bahrani, M. Saeedifard, A. Karimi, and A. Rufer, "Multivariable control of single-inductor dual-output buck converters," *IEEE Trans. Power Electron.*, vol. 29, no. 4, pp. 2061–2070, Apr. 2014.
[43] B. Bahrani, A. Karimi, B. Rey, and A. Rufer, "Decoupled dq-current control of grid-tied voltage source converters using nonparametric models," *IEEE Trans. Ind. Electron.*, vol. 60, no. 4, pp. 1356–1366, Apr. 2012.

Guoqing Gao (Student Member, IEEE) received the B.S. degree in electrical engineering from Xidian University, Xi'an, China, in 2017. He is currently working toward the M.S. degree at the State Key Laboratory of Electrical Insulation and Power Equipment, School of Electrical Engineering, Xi'an Jiaotong University, Xi'an.

His research interests include the modeling and control of dc–dc converters and the renewable energy system.

Wanjun Lei (Member, IEEE) received the B.S., M.S., and Ph.D. degrees in electrical engineering from Xi'an Jiaotong University, Xi'an, China, in 2000, 2004, and 2008, respectively.

He is currently an Assistant Professor with the School of Electrical Engineering, Xi'an Jiaotong University. His research interests include active power filters, power electronics inverters, reactive power compensation, and power quality control techniques.

Dr. Lei is a member of the China Power Supply Society.

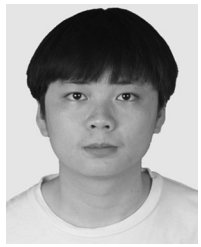

Qibo Tang was born in Guangxi, China, in 1997. He received the B.S. degree in electrical engineering from Chongqing University, Chongqing, China, in 2018. He is currently working toward the M.S. degree in electrical engineering at Xi'an Jiaotong University, Xi'an, China.

His research interests include wireless power transfer, high power density dc–dc converters, and SiC driver control techniques.

Zhongxiu Xiao received the B.S. degree in electrical engineering from North China Electric Power University, Baoding, China, in 2019. She is currently working toward the M.S. degree at the State Key Laboratory of Electrical Insulation and Power Equipment, School of Electrical Engineering, Xi'an Jiaotong University, Xi'an.

Her research interests include the modeling and control of single-phase inverters and dc-dc converters.

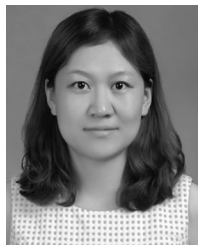

Xiufang Hu received the B.S. degree in electrical engineering from Xi'an Polytechnic University, Xi'an, China, in 2012. She is currently working toward the Ph.D. degree in electrical engineering at Xi'an Jiaotong University, Xi'an.

Her research interests include modeling and control of wireless power transfer systems.

Yue Wang (Member, IEEE) received the B.S. degree from Xi'an Jiaotong University, Xi'an, China, in 1994, the M.S. degree from Beijing Jiaotong University, Beijing, China, in 2000, and the Ph.D. degree from Xi'an Jiaotong University in 2003, all in electrical engineering.

He is currently a Full Professor with the School of Electrical Engineering, Xi'an Jiaotong University. His research interests include wireless power transfer, active power filters, multilevel converters, and HVdc.